



**UNIVERSIDAD DE INVESTIGACIÓN DE
TECNOLOGÍA EXPERIMENTAL YACHAY TECH**

Escuela de Ciencias Químicas e Ingeniería

**TÍTULO: Adsorption of chromium (VI) from aqueous solution
onto natural adsorbents based on Ecuadorian zeolite and
xanthan gum polysaccharide.**

Trabajo de integración curricular presentado como requisito para la
obtención del título de Química

Autor:

Lisandra Estefanía Bastidas Montero

Tutor:

PhD. Ernesto Bastardo - González

Urcuquí, Julio 2020

SECRETARÍA GENERAL
(Vicerrectorado Académico/Cancillería)
ESCUELA DE CIENCIAS QUÍMICAS E INGENIERÍA
CARRERA DE QUÍMICA
ACTA DE DEFENSA No. UITEY-CHE-2020-00040-AD

A los 17 días del mes de julio de 2020, a las 09:00 horas, de manera virtual mediante videoconferencia, y ante el Tribunal Calificador, integrado por los docentes:

Presidente Tribunal de Defensa Dra. LOPEZ GONZALEZ, FLORALBA AGGENY , Ph.D.

Miembro No Tutor Dr. CAETANO SOUSA MANUEL , Ph.D.

Tutor Dr. BASTARDO GONZÁLEZ, ERNESTO LUIS , Ph.D.

El(la) señor(ita) estudiante **BASTIDAS MONTERO, LISANDRA ESTEFANIA**, con cédula de identidad No. **0923569867**, de la **ESCUELA DE CIENCIAS QUÍMICAS E INGENIERÍA**, de la Carrera de **QUÍMICA**, aprobada por el Consejo de Educación Superior (CES), mediante Resolución **RPC-SO-39-No.456-2014**, realiza a través de videoconferencia, la sustentación de su trabajo de titulación denominado: **Adsorption of hexavalent chromium from aqueous solution onto natural adsorbents based on Ecuadorian zeolite and xanthan gum polysaccharide**, previa a la obtención del título de **QUÍMICO/A**.

El citado trabajo de titulación, fue debidamente aprobado por el(los) docente(s):

Tutor Dr. BASTARDO GONZÁLEZ, ERNESTO LUIS , Ph.D.

Y recibió las observaciones de los otros miembros del Tribunal Calificador, las mismas que han sido incorporadas por el(la) estudiante.

Previamente cumplidos los requisitos legales y reglamentarios, el trabajo de titulación fue sustentado por el(la) estudiante y examinado por los miembros del Tribunal Calificador. Escuchada la sustentación del trabajo de titulación a través de videoconferencia, que integró la exposición de el(la) estudiante sobre el contenido de la misma y las preguntas formuladas por los miembros del Tribunal, se califica la sustentación del trabajo de titulación con las siguientes calificaciones:

Tipo	Docente	Calificación
Tutor	Dr. BASTARDO GONZÁLEZ, ERNESTO LUIS , Ph.D.	10,0
Miembro Tribunal De Defensa	Dr. CAETANO SOUSA MANUEL , Ph.D.	9,7
Presidente Tribunal De Defensa	Dra. LOPEZ GONZALEZ, FLORALBA AGGENY , Ph.D.	10,0

Lo que da un promedio de: **9.9 (Nueve punto Nueve)**, sobre 10 (diez), equivalente a: **APROBADO**

Para constancia de lo actuado, firman los miembros del Tribunal Calificador, el/la estudiante y el/la secretario ad-hoc.

Certifico que en cumplimiento del Decreto Ejecutivo 1017 de 16 de marzo de 2020, la defensa de trabajo de titulación (o examen de grado modalidad teórico práctica) se realizó vía virtual, por lo que las firmas de los miembros del Tribunal de Defensa de Grado, constan en forma digital.

BASTIDAS MONTERO, LISANDRA ESTEFANIA
Estudiante

Dra. LOPEZ GONZALEZ, FLORALBA AGGENY , Ph.D.
Presidente Tribunal de Defensa

Dr. BASTARDO GONZÁLEZ, ERNESTO LUIS , Ph.D.
Tutor

Dr. CAETANO SOUSA MANUEL , Ph.D.
Miembro No Tutor

ESCOBAR LANDAZURI, ANA MARIA
Secretario Ad-hoc

AUTORÍA

Yo, **LISANDRA ESTEFANÍA BASTIDAS MONTERO**, con cédula de identidad 0923569867, declaro que las ideas, juicios, valoraciones, interpretaciones, consultas bibliográficas, definiciones y conceptualizaciones expuestas en el presente trabajo; así como, los procedimientos y herramientas utilizadas en la investigación, son de absoluta responsabilidad de el/la autora (a) del trabajo de integración curricular. Así mismo, me acojo a los reglamentos internos de la Universidad de Investigación de Tecnología Experimental Yachay.

Urcuquí, Julio 2020



Lisandra Estefanía Bastidas Montero

CI: 0923569867

AUTORIZACIÓN DE PUBLICACIÓN

Yo, **LISANDRA ESTEFANÍA BASTIDAS MONTERO**, con cédula de identidad 0923569867, cedo a la Universidad de Investigación de Tecnología Experimental Yachay, los derechos de publicación de la presente obra, sin que deba haber un reconocimiento económico por este concepto. Declaro además que el texto del presente trabajo de titulación no podrá ser cedido a ninguna empresa editorial para su publicación u otros fines, sin contar previamente con la autorización escrita de la Universidad.

Asimismo, autorizo a la Universidad que realice la digitalización y publicación de este trabajo de integración curricular en el repositorio virtual, de conformidad a lo dispuesto en el Art. 144 de la Ley Orgánica de Educación Superior

Urcuquí, Julio 2020.

A handwritten signature in blue ink that reads "Lisandra Bastidas". The signature is written in a cursive style with a large, stylized initial 'L' and 'B'.

Lisandra Estefanía Bastidas Montero

CI: 0923569867

DEDICATION

To my family and my dear son.

You are my source of inspiration.

Lisandra Estefanía Bastidas Montero

ACKNOWLEDGMENTS

First and foremost, I would like to express my deepest gratitude to my tutor PhD. Ernesto Bastardo-González for his valuable time, guidance, advice, motivation, encouragement, and constant help throughout this research. It has been a pleasure for me to work with him.

My greatest gratitude is extended to my teachers PhD. Manuel Caetano, and MSc. Lola de Lima, for their contribution to this study and for their valuable recommendations.

I am thankful to PhD. Efrain Rubio for the support received through the research internship I realized at “Centro Universitario de Vinculación y Transferencia de Tecnología” of the BUAP university in Mexico – thank you to PhD. José Ángel Rivera for making this possible and for his help in the early stages of this thesis.

My sincerely thanks to the “Venezuelan Institute of Scientific Research, especially to the “Laboratory of Physical Chemistry of Surfaces” for its contribution to this project.

My special thanks to my friends Gloria, Clara, Cynthia and Jorge for accompanying me through this wonderful university experience and supporting me when I needed it.

Lastly, I remain ever grateful to my parents Laura Montero and Edwin Bastidas for their patience, support, understanding and encouragement in reaching my dreams. My wonderful sisters Laura and Josseline and truly loving son Samuel have been a great source of support and strength with their unconditional love and encouragement.

Lisandra Estefanía Bastidas Montero

RESUMEN

Las zeolitas y los compósitos a base de zeolitas han atraído el interés de varios investigadores como potenciales adsorbentes para la eliminación de iones de metales pesados. El cromo hexavalente se ha identificado como un metal pesado tóxico de gran riesgo para la salud pública, por lo tanto, su disposición indiscriminada representa una amenaza para los humanos y la vida silvestre. En este trabajo, se propone el uso de una zeolita mordenita natural ecuatoriana activada con una solución de H₂SO₄ 98% para mejorar su potencial para la adsorción. Se prepararon tres compuestos con diversas proporciones en masa de zeolita: goma xantana (20:1, 10:1, 5:1) y se caracterizaron mediante varias técnicas incluyendo FTIR, XRD, y SEM/EDS. Se realizaron experimentos para evaluar la eficiencia de los adsorbentes en la remoción de Cr(VI) a partir de soluciones acuosas. También se investigó el efecto del pH, tiempo de contacto y concentración inicial en el proceso de adsorción de Cr(VI). Los modelos de Langmuir, Freundlich y Temkin se utilizaron para caracterizar los datos experimentales y evaluar el comportamiento de adsorción de Cr(VI) de cada adsorbente. La isoterma de Freundlich fue el modelo que mejor describió los datos experimentales para todos los adsorbentes evaluados. Los resultados muestran que las interacciones adsorbato-adsorbente entre la especie Cr(VI) cargada negativamente y los sitios de adsorción protonados de la superficie adsorbente estuvieron involucrados en el proceso de adsorción. La capacidad de adsorción máxima de Cr(VI) fue 0.074 mg/g para el compósito más óptimo con una relación 10: 1 de zeolita: goma-xantana.

Palabras clave: mordenita, goma xantana, isotermas de adsorción, cromo hexavalente.

ABSTRACT

Zeolites and zeolite based composites have attracted interest of several researchers as potential adsorbents for heavy metals ions removal. Hexavalent chromium has been identified as a potential toxic heavy metal of great public health risk, therefore, its indiscriminate disposal represents a threat to humans and wildlife. In this work, the use of a Ecuadorian natural mordenite zeolite is suggested, which was activated with 98% H_2SO_4 to enhance its adsorption potential. Three composites with various mass ratios of zeolite:xanthan gum (20:1, 10:1, 5:1) were prepared and characterized by FTIR, XRD, and SEM/EDS techniques. Laboratory experiments were conducted to investigate the efficiency of adsorbents in the uptake of Cr(VI) from aqueous solutions. The effect of pH, contact time and initial concentration was also investigated. The Langmuir, Freundlich and Temkin isotherm models were used to characterize the experimental data and to assess the adsorption behavior of adsorbents for Cr (VI). The Freundlich isotherm was the best fitted model for describing the experimental data. The results exhibit that adsorbate-adsorbent interactions between the negatively charged Cr(VI) species and the protonated adsorption sites of the adsorbent surface were involved in the adsorption process. The maximum adsorption capacity for Cr(VI) reached was 0.074 mg/g for the 10:1 ratio of zeolite:xanthan gum composite, which was the most optimal.

Keywords: mordenite, xanthan gum, adsorption isotherms, hexavalent chromium.

INDEX

LIST OF TABLES	1
LIST OF FIGURES	2
Chapter 1	3
1.1 Problem Statement.....	3
1.2 Aim and Objectives	5
1.2.1 General Objective	5
1.2.2 Specific Objectives	5
Chapter 2	7
2.1 Heavy metals removal technologies	7
2.1.1 Ion exchange.....	7
2.1.2 Adsorption	8
2.1.3 Adsorption Equilibrium.....	8
2.2 Zeolites	10
2.2.1 Classification	12
2.2.2 Natural zeolites	13
2.3 Xanthan Gum polysaccharide.....	15
2.3.1 Structure	15
2.3.2 Applications.....	16
2.4 Characterization techniques.....	17
2.4.1 X-Ray Diffraction (XRD).....	17
2.4.2 Fourier Transform Infrared Spectroscopy (FT-IR)	18
2.4.3 SEM/EDS analysis	18
Chapter 3	20

3.1	Materials	20
3.2	Samples preparation	20
3.2.1	Zeolite.....	20
3.2.2	Zeolite-Xanthan gum composites.....	21
3.3	Adsorption analysis	22
3.3.1	Synthetic Cr(VI) solutions preparation.....	22
3.3.2	Effect of initial pH.....	22
3.3.3	Effect of contact time	23
3.3.4	Cr(VI) uptake studies	23
3.4	Determination of hexavalent chromium.....	23
3.5	Characterization of zeolite and composites	25
3.5.1	X-Ray Diffraction (XRD).....	25
3.5.2	SEM/EDS	25
3.5.3	Fourier Transform Infrared Analysis (FTIR)	25
Chapter 4	26
4.1	Characterization of the adsorbents	26
4.1.1	X-ray Diffraction Analysis	26
4.1.2	SEM/EDS Analysis	28
4.1.3	Fourier Transform Infrared Spectroscopy (FTIR).....	30
4.2	Adsorption	33
4.2.1	Effect of initial pH on chromium adsorption	33
4.2.2	Effect of contact time	35
4.2.3	Effect of initial concentration	36
4.2.4	Adsorption isotherms.....	36
Chapter 5	41
5.1	Conclusion.....	41

5.2 Suggestions for future work	41
REFERENCES	43

LIST OF TABLES

<i>Table 1. Maximum permissible limits of chromium (VI)</i>	<i>4</i>
<i>Table 2. Zeolite classification scheme developed by Breck (1974) based on SBU's.</i>	<i>12</i>
<i>Table 3. Zeolite:XG ratio of composites.</i>	<i>21</i>
<i>Table 4. Isotherm parameters for Cr(VI) adsorption onto zeolite and zeolite-xanthan gum composites.</i>	<i>37</i>
<i>Table 5. Maximum adsorption capacity of various adsorbents for Cr(VI) removal from aqueous solutions ..</i>	<i>39</i>

LIST OF FIGURES

<i>Figure 1. Primary building units in zeolite structure (a) Tetrahedron with Si (filled circle) at center and O atoms (open circles) at apexes. (b) tetrahedron with Al atom substituting for Si and attached monovalent cation compensating the negative charge (c) tetrahedron chain with divalent cation compensating the charge imbalance between Si and Al. (Note. Taken from Natural and synthetic zeolites, by R.A. Clifton, 1987³⁷.)..</i>	11
<i>Figure 2. (a) Mordenite sheet (100) formed by six membered rings; half of the tetrahedral apices are directed upwards and half are directed downwards. (b) The mordenite (MOR) framework projected along the c-axis. (Note. Taken from “Crystal structures of natural zeolites” by T. Armbruster, and M. Gunter, 2001, Rev. Mineral. Geochemistry⁴²).....</i>	14
<i>Figure 3. Structure of extracellular polysaccharide Xanthan Gum. (Note. Taken from “Xanthan gum: Production, recovery, and properties” by F. García-Ochoa, V. Santos, J. Casas & E. Gómez, 2000, Biotechnol. Adv.⁴⁹).....</i>	16
<i>Figure 4. Geometrical condition for diffraction from lattice planes. (Note. Taken from “X-Ray Diffraction (XRD) Techniques for Materials Characterization” by J. Epp, 2016⁵⁴).....</i>	17
<i>Figure 5. Experimental process of zeolite and Xanthan gum composites preparation.....</i>	22
<i>Figure 6. Cr(VI) calibration curve</i>	24
<i>Figure 7. XRD pattern corresponding to zeolite with two principal phases identified: Mordenite which is highlighted by its respective Miller indices and α-quartz (Q) phase.</i>	26
<i>Figure 8. Xanthan gum XRD pattern</i>	27
<i>Figure 9. XRD patterns of (a) zeolite, and composites (b) COMP 20:1 (c) COMP 10:1 (d) COMP 5:1.....</i>	28
<i>Figure 10. SEM micrograph of zeolite. (Magnification: 5000x)</i>	29
<i>Figure 11. SEM micrograph of composite Comp 20:1 and Comp 10:1.....</i>	29
<i>Figure 12. EDS for (a) zeolite and composites: (b) COMP 20:1, (c) COMP 10:1</i>	30
<i>Figure 13. FTIR spectrum of the natural mordenite sample.</i>	30
<i>Figure 14. FTIR spectrum of xanthan gum.</i>	31
<i>Figure 15. FTIR spectra of COMP 20:1, COMP 10:1, COMP 5:1</i>	32
<i>Figure 16. Effect of initial pH on Cr(VI) removal efficiency (adsorbent dosage: 10 g/L, initial Cr(VI) concentration: 100 mg/L and reaction time: 24 h).....</i>	34
<i>Figure 17. Percentage of removal of Cr (VI) ions by zeolite, COMP(5:1), COMP(10:1) and COMP(20:1) as a function of time. (Initial Cr(VI) concentration: (A) 100 mg/L, (B) 200 mg/L, (C) 300 mg/L, (D) 400 mg/L, (E) 500 mg/L, adsorbent dosage: 10 g/L, and pH: 2)</i>	36
<i>Figure 18. Effect of the initial Cr(VI) concentration (100 - 500 mg/L) in the adsorption capacity (mg/g) and removal efficiency (R %) of Cr(VI) ions (adsorbent dosage: 10 g/L, pH: 2 and reaction time: 24 h).</i>	36
<i>Figure 19. Linear plot of Freundlich isotherm for the adsorption of Cr(VI) ions on (A) Zeolite, (B) COMP 20:1, (C) COMP 10:1 and (D) COMP 5:1 (adsorbent dosage: 10 g/L, Initial Cr(VI) solution concentration: 100 – 500 mg/L, pH: 2 and reaction time: 24 h).....</i>	39

CHAPTER 1

INTRODUCTION

1.1 Problem Statement

Water is the most widely distributed substance on our planet which plays a vital role in preserving life. As human populations and economies grow, not only the demand for freshwater is intensified but also the water resources become exhausted or contaminated decreasing availability of this resource ^{1,2}.

The accumulation of hazardous inorganic and organic contaminants in the environment is a result of unsustainable anthropogenic activities. The indiscriminate disposal of heavy metals has become a major issue that has created global concern. Heavy metals represent a potential risk to wildlife and humans owing to their high toxicity, persistence and bioaccumulation in the environment ^{3,4}. Among them, arsenic, cadmium, chromium, lead and mercury have been identified as the five priority metals of great public health risk. Exposure to these toxic metals, is related to multiple organ damage and cancer in humans and animals ⁵.

The wastewater discharges from several industries contains a large amount of Cr(III) and Cr(VI), being Cr(VI) a non-biodegradable, mutagenic and toxic specie, even at low levels of exposure ⁶. It may enter the human body through food, water, air or absorption through the skin when it come in contact with humans in agriculture, manufacturing, pharmaceutical, industrial or residential settings⁷. According to the World Health Organization (WHO), the maximum concentration permitted in wastewaters of Cr(III) and Cr(VI) are 0.5 mg/L and 0.05 mg/L ,respectively ⁸. In Ecuador, there have been different cases of water contamination by chromium (VI), one case was detected in a study by “The National Irrigation Institute” in a field of Izamba, Ambato. The communities around Ambato and Pachanlica rivers are affected due to the deposition of wastewaters produced by clothing, paper, food and tannery industries ⁹.

Most countries have recognized that the risks related to water and the competition for water resources have increased in the last 2 decades which could compromise the fulfillment of one of the United Nations Sustainable Development Goals (SDGs). In 2015, the United Nations General Assembly set as its 6th goal: “Ensure the availability and

sustainable management of water and sanitation for all.” In order to achieve this purpose and to ensure water security, a better planning and management of water resources is necessary and mandatory ¹⁰. Specifically, contamination of aquatic ecosystems by toxic heavy metals requires great attention in order to reduce their impact in the environment and the risk of adverse health effects.

For this reason, in Ecuador, the “Environmental Quality and Effluent Discharge Standard: Water Resource” dictated under the protection of the “Environmental Management Law and its Regulations” has the objective of protect the quality of water resource to safeguard the health and integrity of people and ecosystems. For different cases, the standard regulates the maximum permissible limits of some chemical compounds. Table 1 shows the maximum limits for chromium (VI) ¹¹.

Table 1. Maximum permissible limits of chromium (VI)

Case	Maximum permissible limits (mg/L)
For water for human consumption and domestic use that only require conventional treatment	0.05
For waters for agricultural use	0.1
For Livestock waters	1.0
Discharge limits to the sewer system	0.5
Discharge limits to a freshwater body	0.5
Discharge limits to a body of seawater	0.5

In order to accomplish the established limits various techniques have been developed for removing heavy metal ions from aqueous solutions, including adsorption, ion exchange, liquid-liquid extraction, reverse osmosis, chemical precipitation, filtration, and

electrochemical methods ¹². Among them, adsorption is the most studied and commonly used method in the industries due to its low-cost, high efficiency and flexibility of technology ¹³. A wide range of materials are available for such process, among which zeolites and zeolite-based materials are considered potential adsorbents with many advantages such as reduced cost, great availability in nature, good mechanical and thermal properties, and high adsorption capacity. Also, natural zeolites do not introduce further pollution into the ecosystems. ¹⁴. For the reasons mentioned above zeolites have been extensively used as adsorbents for the removal of metal ions in the treatment of industrial and urban wastewaters ^{12,14,15}. In the last decade, novel and alternative options are being developed to potentiate the properties of zeolites and increase their applications ¹⁶. Xanthan gum (XG) have recently attracted an increasing research interest due to it can be used to synthesize polymer-inorganic hybrid composites with high adsorption capacity and operation stability. The major advantages of XG are that it is biodegradable, and has carboxyl and hydroxyl functional groups that may serve as active sites for heavy metals adsorption ^{17,18}.

1.2 Aim and Objectives

1.2.1 General Objective

The main objective of this work was to study the removal of Cr (VI) metal ions from aqueous solutions by adsorption using natural mordenite zeolite and zeolite – xanthan gum polysaccharide composites.

1.2.2 Specific Objectives

For the fulfillment of the main objective, the following specific objectives were formulated:

- Prepare three composites containing activated zeolite and xanthan gum with mass ratios 20:1, 10:1, and 5:1.
- Characterize the natural zeolite and zeolite – xanthan gum composites with various techniques including FTIR, SEM-EDS, and DRX.
- Conduct adsorptions experiments in order to evaluate the Cr(VI) adsorption capacity onto prepared adsorbents.

- Analyze the effect of pH, contact time and initial concentration on the performance of the adsorbents.
- Determine the initial and final concentration of Cr(VI) ions during the adsorption process by UV-Vis spectroscopy.
- Explore the possible adsorption mechanism by adsorption isotherms models.

CHAPTER 2

THEORETICAL FRAMEWORK

2.1 Heavy metals removal technologies

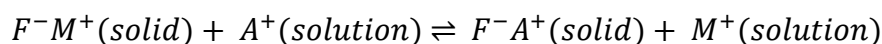
As it was discussed before, industrial waste discharge is one of the major problems affecting the environmental and public health, hence it has been of significant concern the development of remediation technologies for removing contaminants from effluents. The most commonly available methods used for this purpose are: membrane separation, chemical oxidation and reduction, precipitation, filtration, electrochemical treatment, ion exchange and adsorption^{19,20}. Although most of these technologies have great potential for removal of metals, they also require expensive operational costs and generate large amounts of toxic sludge requiring further treatment and controlled final disposal^{21,22}. Adsorption by natural adsorbents present some advantages among the high - techniques due to its efficiency, availability in large quantities and economical aspects²³. Moreover, ion exchange has been used frequently as a convenient method too.

2.1.1 Ion exchange

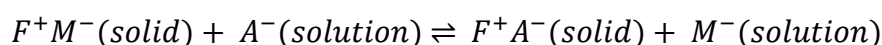
Ion exchange process is the reversible interchange of ions between a solid phase (ion exchanger) and a solution phase. Ion exchanger is usually insoluble in the medium in which the exchange reaction takes place. The ion exchanger can be cation exchanger having a negative charge that exchange cations or anion exchanger which possesses a transferrable anion with an immovable cation²⁴.

Ion reactions can be represented by the following equations:

For cation exchange:



For anion exchange:



where F is the insoluble fixed ion carrying M as the exchange ions .

Ion exchange can be used in different treatment processes such as purification, separation and decontamination. It is mainly applied in the purification and demineralization of water²⁵. High cation exchange capacity of natural and synthesized clays, zeolites and resins have been extensively used for the uptake of metals from aqueous solutions. However, this method has certain disadvantages, for instance it is limited to certain concentration of metals in the solution, specific temperature and pH⁷.

2.1.2 Adsorption

Adsorption is a process in which a substance (molecules, atoms or ions from gas or liquid) is attracted and accumulated on a solid surface. The substance on which the adsorption takes place is called *adsorbent* and the substance which gets adhered is known as *adsorbate*. This process is based on the interaction between the fields of forces of both surfaces when are brought into contact. According to the nature of the forces involved in the adsorption process, it can be classified into: physical and chemical adsorption²⁶.

- *Physical adsorption* occurs when the adsorbate is bound to the surface of the adsorbent by van der Waals interactions²⁶. It is a reversible process due to it involves the formation of weak bonds which can be easily broken, that is, desorption process can take place at the same temperature of adsorption,²⁷.
- *Chemical adsorption* takes place when electrons are exchanged or shared between the adsorbate molecules and adsorbent surface resulting in the formation of a strong chemical bond. Chemisorption is a specific phenomenon, which occurs in certain areas of the solid known as active centers resulting in a slow and irreversible process^{26,27}.

2.1.3 Adsorption Equilibrium

The adsorption equilibrium can be defined as the state in which the rates at which solute molecules are adsorbed and desorbed onto a surface are equal, that is, the molecules striking to the surface are in dynamic equilibrium with the adsorbed molecules rebounding from the surface.²⁶. The adsorption equilibrium is characteristic of each system and can be approached through adsorption isotherms²⁷.

2.1.3.1 Adsorption Isotherms

Adsorption isotherms are isothermal relationships between the amount of solute adsorbed per unit mass of adsorbent in the solution and equilibrium concentration²⁸. These equations are used to describe the mechanism of adsorption, surface properties and the degree of interaction or affinity between adsorbate and adsorbent²⁹.

2.1.3.1.1 Langmuir Isotherm

The Langmuir isotherm model assumes a homogenous adsorption process with the formation of a monolayer surface phase. Other assumptions in which this model is based are (a) there are a fixed number of adsorption sites, (b) one sorbate molecule reacts with only one active site, (c) no interaction between the sorbate species. The Langmuir adsorption model can be expressed as Eq (1)^{30,31}:

$$q_e = \frac{q_{max} \cdot k_L}{(1 + k_L \cdot C_e)} \quad (1)$$

which can be expressed in the linearized form as Eq (2):

$$\frac{C_e}{q_e} = \frac{1}{k_L \cdot q_{max}} + \frac{1}{q_{max}} \cdot C_e \quad (2)$$

where q_e (mg/g) is the amount of adsorbed metal ions per unit weight of adsorbent and C_e (mg/L) is the concentration of free metal ions in solution, k_L is the Langmuir adsorption constant that indicates affinity of the binding sites (L/mg), and q_{max} is the mono-layer adsorption capacity of adsorbent (mg/g). The constant q_{max} and k_L can be determined by plotting (C_e/q_e) versus C_e .^{32,33}

Adsorption can also be evaluated in terms of separation factor, R_L which is given by Eq (3):

$$R_L = \frac{1}{(1 + k_L \cdot C_o)} \quad (3)$$

If the value of R_L is within the range of 0 and 1, the adsorption is favorable, but if R_L is higher than 1, the adsorption process is considered to be unfavorable²³.

2.1.3.1.2 Freundlich Isotherm

The Freundlich isotherm is an empirical equation used to describe non-ideal and reversible adsorption process on surface adsorption sites which are energetically heterogeneous, not constricted to monolayer formation^{20,33}. The model assumes that the energy of adsorption of a metal binding to an adsorbent site depends on whether or not the adjacent sites are already occupied³⁴. It can be expressed as Eq (4)³⁵:

$$q_e = K_f \cdot C_e^{\frac{1}{n}} \quad (4)$$

where K_f (mg/g) is the Freundlich constant related to adsorption capacity, and n is related to adsorption intensity; values of $n > 1$ represent favorable adsorption conditions²³. Equation (4) may also be expressed in the logarithmic form as Eq (5)³³:

$$\ln q_e = \ln K_f + \frac{1}{n} \cdot \ln C_e \quad (5)$$

The constants K_f and n can be obtained from the slope and intercept of the plot of $\ln q_e$ against $\ln C_e$.

2.1.3.1.3 Temkin Isotherm

Assumes that the absorption heat decrease linearly with coverage and adsorption is characterized by a uniform distribution of binding energy. The linear form of Temkin isotherm is as Eq. (6):

$$q_e = (B \ln k_T) + (B \ln C_e) \quad (6)$$

Where, k_T is the Temkin constant (L/mol)^{23,32}.

2.2 Zeolites

The name zeolite was coined by Fredrik Cronstedt (1756) from two Greek words, $\zeta\epsilon\iota\nu$ = “to boil” and $\lambda\iota\theta\omicron\varsigma$ = “stone”, to describe minerals that seem to boil because they lose water rapidly by heating³⁶. Zeolites are microporous and crystalline aluminosilicates with frameworks that consist of an assemblage of TO_4 tetrahedra (T = Si, Al), linked by sharing oxygen atoms as can be seen from Figure 1. The combination of purely SiO_4 tetrahedral

units leads to the formation of an uncharged solid known as silica (SiO₂). The partial substitution of Si⁴⁺ by Al³⁺ produces a negative charge in the framework, which is compensated by the presence of extraframework cations (usually K⁺, Na⁺, Ca²⁺, and less frequently Li⁺, Mg²⁺, Ba²⁺, Sr²⁺) located together with water molecules in structural channels.

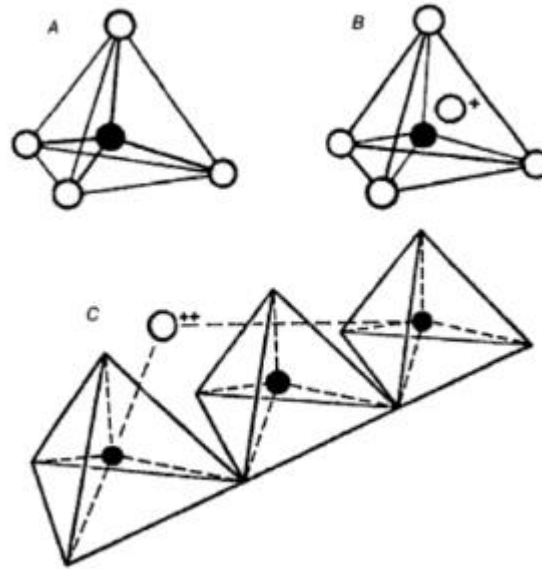
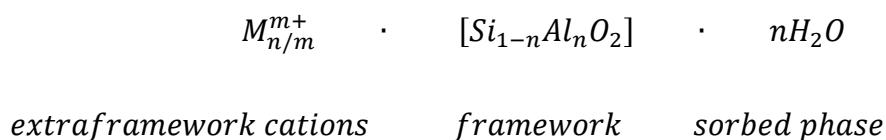


Figure 1. Primary building units in zeolite structure (a) Tetrahedron with Si (filled circle) at center and O atoms (open circles) at apexes. (b) tetrahedron with Al atom substituting for Si and attached monovalent cation compensating the negative charge (c) tetrahedron chain with divalent cation compensating the charge imbalance between Si and Al. (Note.

Taken from *Natural and synthetic zeolites*, by R.A. Clifton, 1987³⁷.)

The zeolite composition can be described as having three relatively independent components (aluminate-silicate framework, exchangeable cations and zeolitic water) as follows^{36,38,39}:



These extraframework cations are commonly exchangeable and give rise to the ion-exchange capacity of these materials. In addition, zeolites are able to lose and gain water reversibly without changing their crystal structure. The most significant feature of the zeolite structure is its microporosity which is a result of the topology of the framework^{38,40}.

In general, zeolites satisfy the following classification rules ³⁹:

- a. Tetrahedrally coordinated framework cations.
- b. Cavity system (channels and cages) in the range of 0.2Å to 20 Å.
- c. Zeolitic water.
- d. Cation-exchange capability.

Rule (a) and (b) are a necessary requisite for a structure type to be a zeolite, while rule (c) and (d) are only fulfilled by true zeolites. The maximum diameters of pore openings known for aluminosilicate - type zeolites is of 7.4 Å (faujasite). In the case of true zeolites, their channel and cage systems possess crystalline properties ³⁹.

2.2.1 Classification

Currently, zeolites can be classified in three different ways. The first is based on the topology of the framework. Up to now, 176 structure types of zeolites have been approved and assigned a three letter code by the Structure Commission of the International Zeolite Association. ⁴¹.

The second scheme of classification is in terms of so-called "Secondary building units (SBU), which are geometric arrangements of TO₄ tetrahedra (the primary building unit for zeolites). According to this classification there are seven major groups established by Breck in 1974 (Table 2) ⁴².

Table 2. Zeolite classification scheme developed by Breck (1974) based on SBU's.

Group 1 (S4R-single-4-ring)	Group 3 (D4R – double 4-ring)	Group 6 (T₈O₁₆)
Analcime	(A, N-A, ZK-4)	Mordenite
Harmotome		Dachiardite

Phillipsite	Group 4 (D6R – double 6-ring)	Ferrierite
Gismondine		Epistilbite
Paulingite		Bikitaite
Laumontite		
Yugawaralite		
(P)	(X, Y, ZK-5, L)	
Group 2 (S6R –single 6-ring)	Group 5 (T₅O₁₀)	Group 7 (T₁₀O₂₀)
Erionite	Natrolite	Heulandite
Offretite	Scolecite	Clinoptilolite
Levynite	Mesolite	Stilbite
Sodalite hydrate	Thomsonite	Brewsterite
(T, Omega)	Gonnardite	
	Edingtonite	

Note 1. Taken from “Crystal structures of natural zeolites” by T. Armbruster, and M. Gunter, 2001, *Rev. Mineral. Geochemistry*⁴².

The third way of classification is similar to the SBU classification type, but it includes historical aspects such as the chronology in which zeolites were discovered and named. It is more commonly used by geologists.⁴²

2.2.2 Natural zeolites

Natural zeolites were discovered more than 200 years ago, and after many studies, the remarkable intrinsic properties of natural zeolites were fully recognized⁴³. Zeolites are found in nature occurring in a wide variety of volcanic and sedimentary rocks^{38,43}. The geological formation of zeolites defines their physical and chemical properties which defines their application and effectiveness in technological processes⁴⁴. There are over 40 known types of naturally occurring zeolites, but only seven of them form large mineable mineral deposits (clinoptilolite-heulandite, mordenite, chabazite, erionite, ferrierite, analcime, philipsite)⁴⁵. Clinoptilolite (HEU) and mordenite (MOR) are two natural zeolites that are widely used for ion exchange agricultural uses and as sorbents³⁸. As natural zeolites

are generally impure they are excluded from commercial applications where high degree of uniformity and purity are needed ⁴⁶.

2.2.2.1 Mordenite zeolite characteristics (MOR)



Orthorhombic

Space Group: Cmcm

a = 18.11 Å

b = 20.46 Å

c = 7.52 (Å)

Henry How (1864) proposed the name *mordenite* based on the location this mineral was found; Morden, King's Co., Nova Scotia. The origin of mordenite may be sedimentary or hydrothermal. Sedimentary mordenites contain the highest Si-content ³⁶.

The mordenite structure can be visualized as sheets built by six-membered rings parallel to (100) plane (Figure 2 a), which are connected by four-membered rings. As a result of this attachment, the hexagonal sheets are deformed becoming corrugated and channels consisting of twelve-membered rings (aperture 6.5 x 7.0 Å) and eight-membered rings are formed parallel to the c-axis (Figure 2 b). The wide channels are connected by another set of compressed eight-membered rings (aperture 2.6 x 5.7 Å) parallel to the b-axis ^{36,42}.

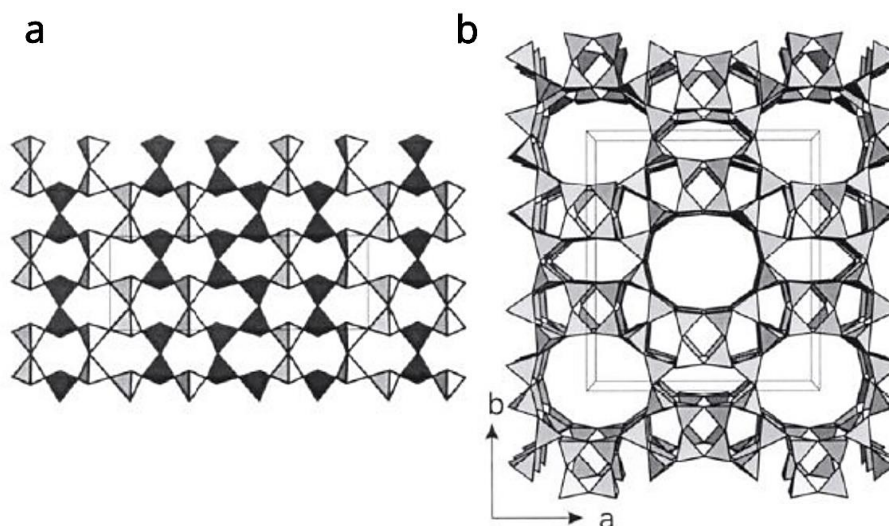


Figure 2. (a) Mordenite sheet (100) formed by six membered rings; half of the tetrahedral apices are directed upwards and half are directed downwards. (b) The mordenite (MOR)

framework projected along the c-axis. (Note. Taken from “Crystal structures of natural zeolites” by T. Armbruster, and M. Gunter, 2001, *Rev. Mineral. Geochemistry* ⁴²)

Mordenite belongs to the category of siliceous zeolite. Mordenite of sedimentary origin has the Si-content at the highest level. The extent of isomorphous substitution of Al for Si in the tetrahedral framework is the source of the ion exchange capacity⁴⁷. Based on theoretical cation exchange capacity (CEC) values and zeolite contents in tuff occurrences, it was determined that mordenite-rich tuffs possesses CEC values ≥ 1.0 meq g⁻¹ with sporadic much higher values, up to 1.8 – 2.0 meq g⁻¹ ⁴⁸. Zeolites selectivity towards cations and anions is an important property in water treatment process⁴⁴. It has been demonstrated the easy ion-exchange of mordenite with all alkali (Cs⁺ > K⁺ > Rb⁺ > Na⁺ > Li⁺) and alkali earth metals (Ba²⁺ > Sr²⁺ > Ca²⁺ > Mg²⁺). Generally, monovalent ions are preferred to divalent ones ^{36,44}. Natural zeolites can be modified by different methods (acid treatment, ion exchange, and surfactant functionalization) in order to increase their adsorption capacity for organic matter and anions ⁴⁴.

2.3 Xanthan Gum polysaccharide

Xanthan gum is a natural polysaccharide of great industrial and commercial importance ⁴⁹. It is secreted by the micro-organism *Xanthomonas campestris*. Commercially, it is produced by a fermentation process ⁵⁰.

2.3.1 Structure

Xanthan gum is a long-chain polysaccharide with a primary structure consisting of a linear backbone of 1,4-linked β -D-glucose units with a high number of trisaccharide side chains on every other glucose at C-3 as it is shown in Figure 3. The trisaccharide side chain is formed by a D-glucuronic acid unit 1,4-linked to a terminal mannose unit and 1,2-linked to a second mannose residue that is attached to the main chain. Approximately 50% of the terminal D-mannose units are pyruvylated with an unknown distribution and the non-terminal mannose residue usually containing an acetyl group at C-6 ⁵⁰. An anionic polysaccharide type is produced due to the presence of acetic and pyruvic acids ⁴⁹.

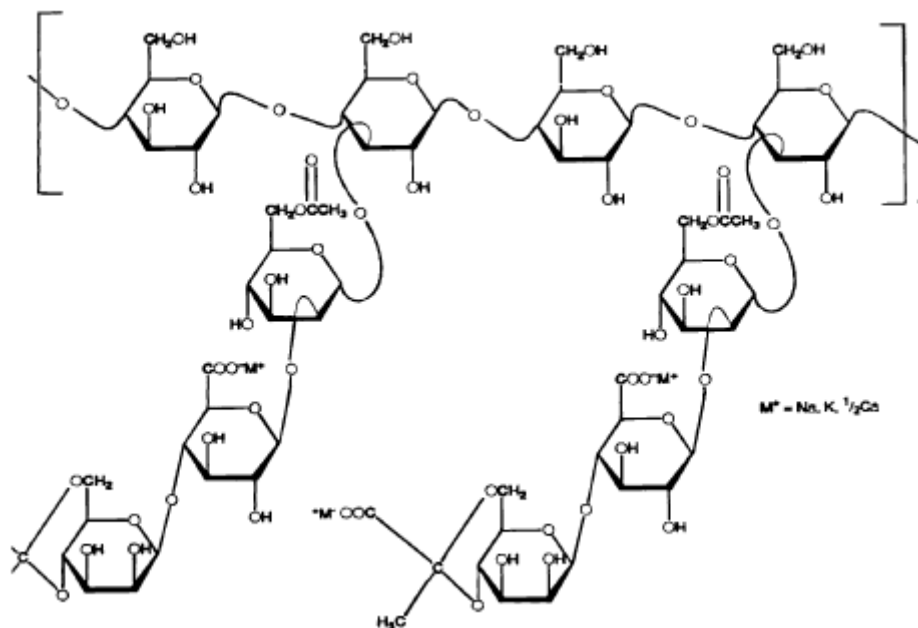


Figure 3. Structure of extracellular polysaccharide Xanthan Gum. (Note. Taken from “Xanthan gum: Production, recovery, and properties” by F. García-Ochoa, V. Santos, J. Casas & E. Gómez, 2000, *Biotechnol. Adv.* ⁴⁹)

Xanthan gum is shown by electron microscopy and X-ray diffraction studies to be a double stranded, right-handed five-fold helix ^{50,51}. In this conformation, the trisaccharide branches are closely aligned with the polymer backbone and stabilize the overall conformation by non-covalent interactions, primarily hydrogen bonding ⁵⁰. The temperature is the main factor that regulates the molecular conformation, structural arrangement and extensional viscosity of Xanthan gum. Upon heating, the xanthan gum double helix chains become dissociated and upon cooling at room temperature, the chains are reversed into helical structure ¹⁸.

2.3.2 Applications

Xanthan gum is used in a wide number of industrial applications owing to its remarkable properties. In the food industry it is used as a stabilizing and thickening agent for some food products ⁵². It plays an important role in the manufacture of agricultural products, cleaners, coatings, paper, cosmetics and pharmaceutical formulations. Xanthan gum has received special attention in the petroleum industry. Due to its rheological properties, high temperature stability and salt compatibility xanthan gum is suitable for enhance oil recovery (EOR) and oil drilling fluids (e.g. oil) processes ^{49,52,53}.

2.4 Characterization techniques

This section describes the methodical techniques that were used for the characterization of zeolite and zeolite-xanthan gum composites prepared. The different samples were characterized using several techniques including: X-ray diffraction (XRD) analysis, Fourier transform infrared spectroscopy (FTIR), scanning electron microscopy (SEM) and Brunauer-Emmet-Teller (BET) surface area analysis.

2.4.1 X-Ray Diffraction (XRD)

Since its discovery in 1912, X-ray diffraction (XRD) by crystals has been the most widely used technique for the study of crystalline materials. The method depends on the wave character of the X-rays and the regular spacing of the planes in a crystal.

W.L. Bragg gave the geometrical interpretation of the XRD phenomenon which is based on wave interferences. X-ray beams incident on a crystalline solid will be diffracted by the crystallographic planes as illustrated in the Figure 4. When the geometrical conditions established by Bragg's law Eq. (7) are satisfied, diffraction occurs.

$$n\lambda = 2d_{hkl}\sin\theta \quad (7)$$

In Eq. 7, n is a constant that represents the order of diffraction, λ is the wavelength of the incident radiation (nm), d_{hkl} is the lattice spacing of the crystal (nm) and θ is the angle of the diffracted beam.

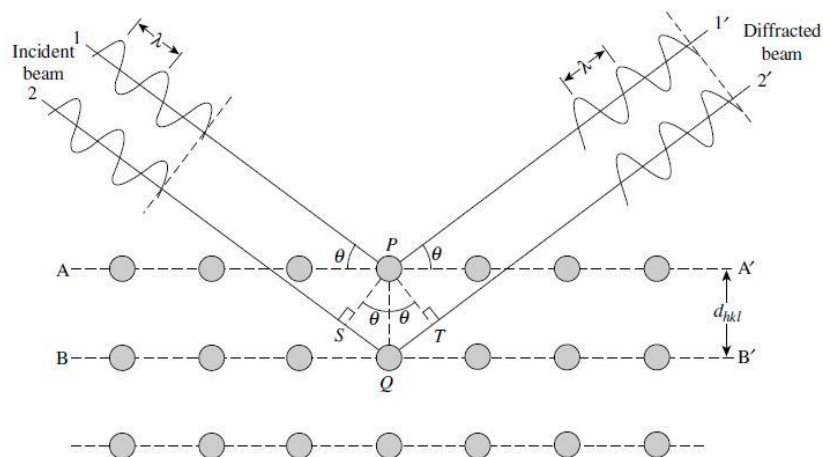


Figure 4. Geometrical condition for diffraction from lattice planes. (Note. Taken from “X-Ray Diffraction (XRD) Techniques for Materials Characterization” by J. Epp, 2016⁵⁴)

The most extensively used X-ray diffraction technique in materials characterization is X-ray powder diffractometry. In this technique a diffractometer is used to detect X-ray diffraction from solids and to record a spectrum of diffraction intensity versus the diffraction angle (2θ). In this instrument, monochromatic X-rays are used, that is, X-rays of a single wavelength. X-ray powder diffractometry allows us to identify the crystal structure and quality of an unknown compound. Based on the principle that X-ray diffraction pattern is unique for each sample, it can be analyzed and compared with a database that contains information of more than 60,000 diffraction spectra of known crystalline substances^{54,55}.

2.4.2 Fourier Transform Infrared Spectroscopy (FT-IR)

Fourier transform infrared spectroscopy is mainly used in the identification of functional groups in many samples (gas, liquid and solid), confirmation of identities and determination of concentration of components in a mixture. The principle of this technique is based on the interaction of infrared light with matter. When the IR radiation is adsorbed by a molecule having an electric dipole, a change in its net dipole moment is caused as a result of its rotational and vibrational motions. Each molecule, depending on the characteristics of their bonds (every bond has their own particular natural vibrational frequency), will absorb IR radiation of a specific wavelength. The fundamental measure obtained by this technique is an infrared spectrum which represents the infrared intensity versus light wavelength. In this way, molecules with different structures will not have the same infrared spectrum, so they can be identified^{56,57}.

2.4.3 SEM/EDS analysis

The scanning electron microscope (SEM) is one of the most versatile instruments available for the examination and analysis of the microstructural characteristics of solids objects. The primary reason for the SEM's usefulness is the high resolution which can be obtained when bulk objects are examined, values of the order of 5 nm are usually quoted for commercial instruments. The SEM is also capable of examining objects at very low magnification. Basically, an electron beam enters the specimen chamber and strikes the specimen at a single location. Within the interaction volume elastic and inelastic scattering occur, producing detectable signals from backscattered electrons, secondary electrons, absorbed electrons, characteristic and continuum X-ray and cathodoluminescent. Local

topography, composition and other facts can be obtained at the single location of the electron beam impact.

CHAPTER 3

EXPERIMENTAL SECTION

3.1 Materials

The mordenite zeolite used throughout this study is originated from a deposit located in the city Isidro Ayora, Guayaquil – Ecuador, and was purchased from the company INDAMI CIA. LTDA. Xanthan gum (XG) was purchased from the company Produquimic, Quito - Ecuador. Barium chloride (BaCl_2), sulfuric acid (H_2SO_4), acetone, potassium chromate, hydrochloric acid (HCl), and sodium hydroxide (NaOH) were of analytical grade.

3.2 Samples preparation

3.2.1 Zeolite

3.2.1.1 Zeolite concentration

For the experimental analysis, a pretreatment was applied to the natural mordenite zeolite. Because of natural zeolites contain a variety of contaminants, including clays, quartz, mica, feldspar, iron and titanium minerals and calcites, the first step involved the separation of the zeolite fraction from the soil sample. In this process, 200 grams of zeolite sample was dispersed into 2L distilled water by magnetic stirring. The suspension was transferred to a 2L graduated cylinder and allowed to stand until mineral phases were separated based on their density property. The zeolite fraction was collected with a pipette and dried at 120 °C for 12 hours (POL EKO oven) before grinding with mortar until a fine powder was obtained. The concentrated zeolite product was calcined (Vulcan A-550 muffle furnace) at 500 °C for 5 hours.

3.2.1.2 Zeolite acid activation

In order to activate the zeolite, the method described by Bastardo, et al.⁵⁸ was carried out with some modifications. In an Erlenmeyer flask 25 g of zeolite was dispersed into 25 mL of distilled water with 20 mL of sulfuric acid (H_2SO_4). The suspension was heated at 90 °C under reflux during 16 hours with constant stirring. Once the activation process ended, the zeolite was recovered through gravity filtration and it was washed with distilled water

until sulfate ions were completely removed. To ensure the absence of sulfates, barium chloride (BaCl₂) solution was added to the supernatant of each wash until there was no reaction (white precipitate formation). Finally, zeolite was dried by oven at 40 °C, pulverized and stored for the next steps.

3.2.2 Zeolite-Xanthan gum composites

In order to prepare zeolite-Xanthan gum composites, the method described by Ahmad and Mirza ¹⁷ was carried out with some adaptations as shown in **¡Error! No se encuentra el origen de la referencia.**Figure 5. In detail, three composites were prepared with the following mass relations (Table 3):

Table 3. Zeolite:XG ratio of composites.

Code	Zeolite : XG ratio	Mass ratio
COMP 20:1	20 : 1	5 g : 0.25 g
COMP 10:1	10 : 1	5 g : 0.5 g
COMP 5:1	5 : 1	5 g : 1 g

Firstly, the indicated mass of zeolite was left for dispersion in distilled water during 48 hours with moderate stirring. The indicated amount of xanthan gum was dissolved in 300 mL of distilled water at 60 °C until a clear solution was obtained. The mixture of zeolite and xanthan gum was left in mild ultrasound sonication for 6 h at 60 °C. The solid was recovered by filtration and dried by oven at 80 °C for 3 hours. Finally, it was powdered in mortar and stored for further studies.

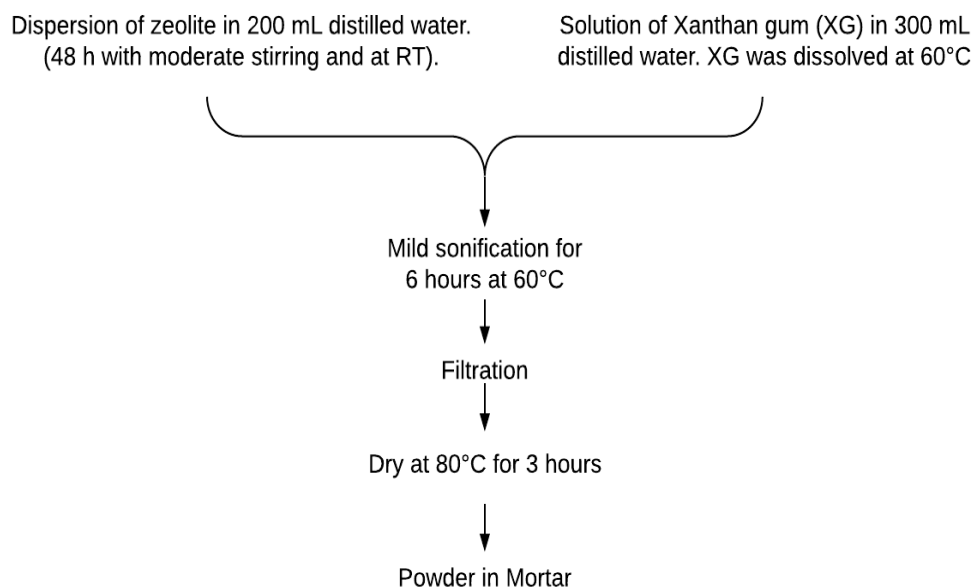


Figure 5. Experimental process of zeolite and Xanthan gum composites preparation.

3.3 Adsorption analysis

3.3.1 Synthetic Cr(VI) solutions preparation

The stock of Cr(VI) ions solution at concentration of 1000 mg/L was prepared by dissolving 3.735 g of potassium chromate (K_2CrO_4) analytical reagent grade into 1 L of distilled water. Experimental solutions of the desired concentrations (100, 200, 300, 400 and 500 mg/L) were obtained by successive dilution. Sodium hydroxide (NaOH) and hydrochloric acid (HCl) were used for pH adjustment and controlled by pH-meter (Mettler Toledo).

3.3.2 Effect of initial pH

The effect of pH solution (pH = 2 and 9) on adsorption of Cr(VI) ions on zeolite and zeolite-xanthan gum composites was determined by agitating 0.1 g of each adsorbent in 10 mL of potassium chromate solution with initial concentration of 100 mg/L. Moderate agitation was given during 24 h contact and at room temperature. The pH of the solutions was adjusted using 1 M HCl and 1 M NaOH and controlled by pH-meter.

3.3.3 Effect of contact time

The effect of time ($t = 3$ and 24 h) on adsorption of Cr(VI) ions on zeolite and xanthan-gum composites was determined by agitating 0.1 g of each adsorbent in 10 mL potassium chromate solution with initial concentration from 100 to 500 mg/L at pH 2 .

3.3.4 Cr(VI) uptake studies

The adsorption studies were carried out using batch adsorption mode, where 0.1 g of adsorbent was dispersed in plastic containers containing 10 mL of different initial concentrations (100 , 200 , 300 , 400 and 500 mg/L) of potassium chromate solutions at pH 2 . All the plastic containers were kept at room temperature with moderate stirring for 24 hours. The suspensions were filtered using N° 42 Whatman paper and the final concentration of the metal ion in the filtrate was analyzed by UV- Visible spectrophotometer as described in the section 3.4.

3.4 Determination of hexavalent chromium

To determine the presence of Cr(VI) in the samples of study, the following procedure was carried out:

Preparation of standards for the calibration curve: Six working standard Cr(VI) solutions with different concentrations (100 , 200 , 300 , 400 , 500 and 600 mg/L) were prepared for calibration. The pH of the solutions was adjusted to 2 by adding nitric acid in order to measure their absorbance. The absorbance of each solution was measured by UV-Vis spectrophotometer PerkinElmer Lambda 1050 at maximum wavelength which resulted at 444 nm. The absorbance values were recorded to build the calibration curve for the adsorption system.

Calibration curve: The calibration curve was constructed by plotting the values of absorbance against concentration (Figure 6). According to the Lambert Beer law, it should be a straight line passing through the origin, i.e. the absorbance (A) is directly proportional to the concentration (c).

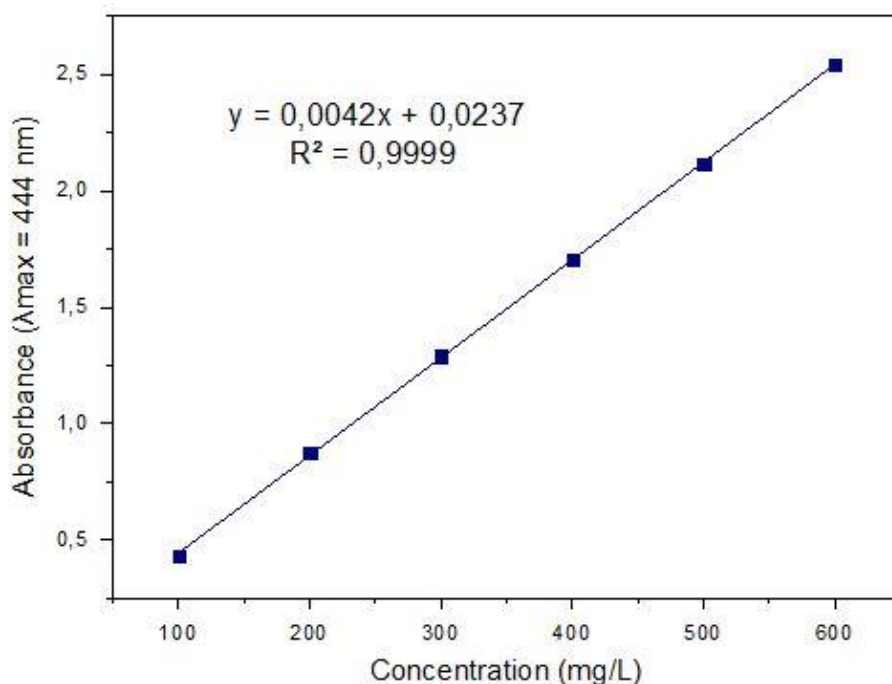


Figure 6. Cr(VI) calibration curve

Protocol for hexavalent chromium determination: Before measuring the absorbance, the experimental samples were acidified with few drops of 98% nitric acid to reach pH 2 in which dichromate formation predominates. The presence of Cr(VI) in the form of dichromate was evidenced by the formation of an orange colored solution. The spectrophotometer reading was at a wavelength of 444 nm. The final concentration of Cr(VI) in the samples was calculated with the equation obtained using the calibration curve.

Adsorption capacity (Q_e) was calculated by the equation (10):

$$Q_e = \frac{(C_o - C_e)V}{W} \quad (10)$$

and the Cr(VI) removal percentage $R\%$ was calculated as follows in the equation (11)

$$R\% = \frac{(C_o - C_e)}{C_o} \times 100 \% \quad (11)$$

where C_o and C_e (mg/L) are the initial and the equilibrium concentration of hexavalent chromium metal ions in aqueous solution, before and after contact. V (L) is the volume of the solution of Cr (VI), W (g) is the weight of adsorbent ⁶.

3.5 Characterization of zeolite and composites

3.5.1 X-Ray Diffraction (XRD)

X ray-diffractometer with CuK α radiation ($\lambda=1.5406 \text{ \AA}$) was used to specify the diffraction pattern of the adsorbents through X-ray powder diffraction technique with 0.02° step size, 0.42 step time and measurement range of $5-80^\circ$. XRD patterns of the samples were obtained using a diffractometer Siemens D-500.

3.5.2 SEM/EDS

SEM technique was used to characterize the surface morphology of the adsorbents. The Scanning Electron Microscopy images and surface composition were obtained at resolutions from 250x to 5000x. Scanning electron micrographs were obtained using a Philips XL-30 Scanning Electron Microscope equipped with a LINK-ISIS-EDS system.

3.5.3 Fourier Transform Infrared Analysis (FTIR)

In order to distinguish the presence of functional groups in the surface of the adsorbents, FT-IR analysis was performed in an FTIR spectrometer by KBr disc technique in the region of $400-4000 \text{ cm}^{-1}$. FTIR spectra of the samples were recorded using a Nicolet model 205 spectrometer.

CHAPTER 4

RESULTS AND DISCUSSION

4.1 Characterization of the adsorbents

4.1.1 X-ray Diffraction Analysis

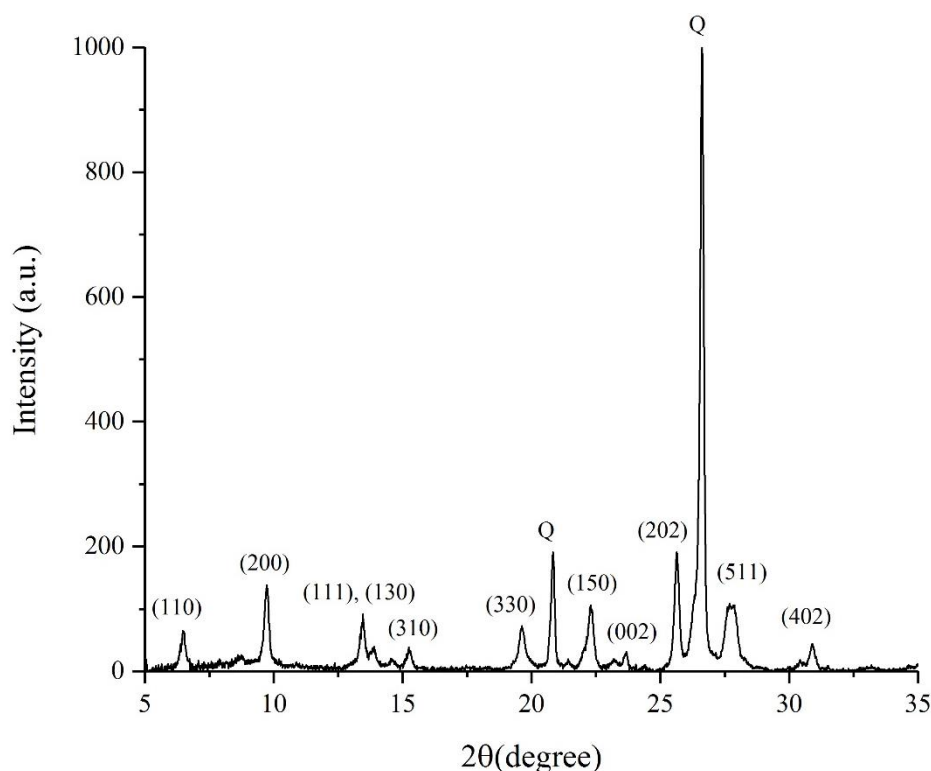


Figure 7. XRD pattern corresponding to zeolite with two principal phases identified: Mordenite which is highlighted by its respective Miller indices and α -quartz (Q) phase.

The X-ray diffraction pattern (XRD) of the activated zeolite sample is given in Figure 7. Sharp signals are observed in the diffraction pattern indicating high crystallinity. The reflections at $2\theta = 6.47^\circ, 9.74^\circ, 13.43^\circ, 13.84^\circ, 15.26^\circ, 19.59^\circ, 22.22^\circ, 23.66^\circ, 25.60^\circ, 27.61^\circ$ and 30.84° are characteristic of mordenite type zeolite with orthorhombic structure according to the standard JCPDS file card number (80-0643), and it is in good agreement with a zeolite of idealized structure $(\text{Na}_2, \text{Ca}, \text{K}_2)_4(\text{Si}_{40}\text{Al}_8)\text{O}_{96} \cdot 28\text{H}_2\text{O}$. The XRD pattern also shows evidence of the presence of quartz (α - SiO_2), which could not be removed during the concentration treatment, showing characteristic reflections at $2\theta = 20.80^\circ$, and 26.63° (JCPDS card number 03-0419). Quartz is considered as a natural impurity in this type of materials.

XRD pattern of xanthan gum is presented in Figure 8 which presents two broad reflections centered around 20 and 37°/2θ confirming its amorphous nature. The results are in accordance with the literature data for xanthan gum ⁵⁹.

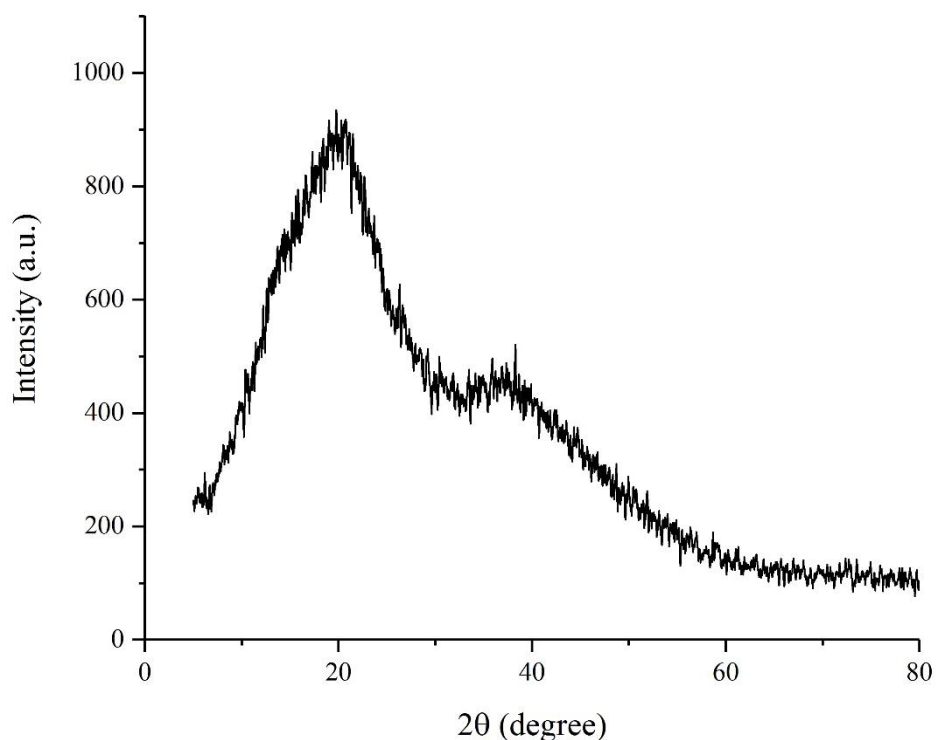


Figure 8. Xanthan gum XRD pattern

The Figure 9 shows the comparison between the XRD patterns of activated zeolite and zeolite-xanthan gum composites. In general, all composites exhibit similar diffraction pattern to the zeolite precursor. The amorphous phase related to xanthan gum is not observed in the XRD pattern of composites due to its low scattering in comparison to the much more crystalline zeolite, as previously reported on composites of zeolite-xanthan gum by other authors ^{17,18}. In addition, the position of the diffraction reflections did not change significantly, which means that the incorporation of xanthan gum did not change the structure of the zeolite itself.

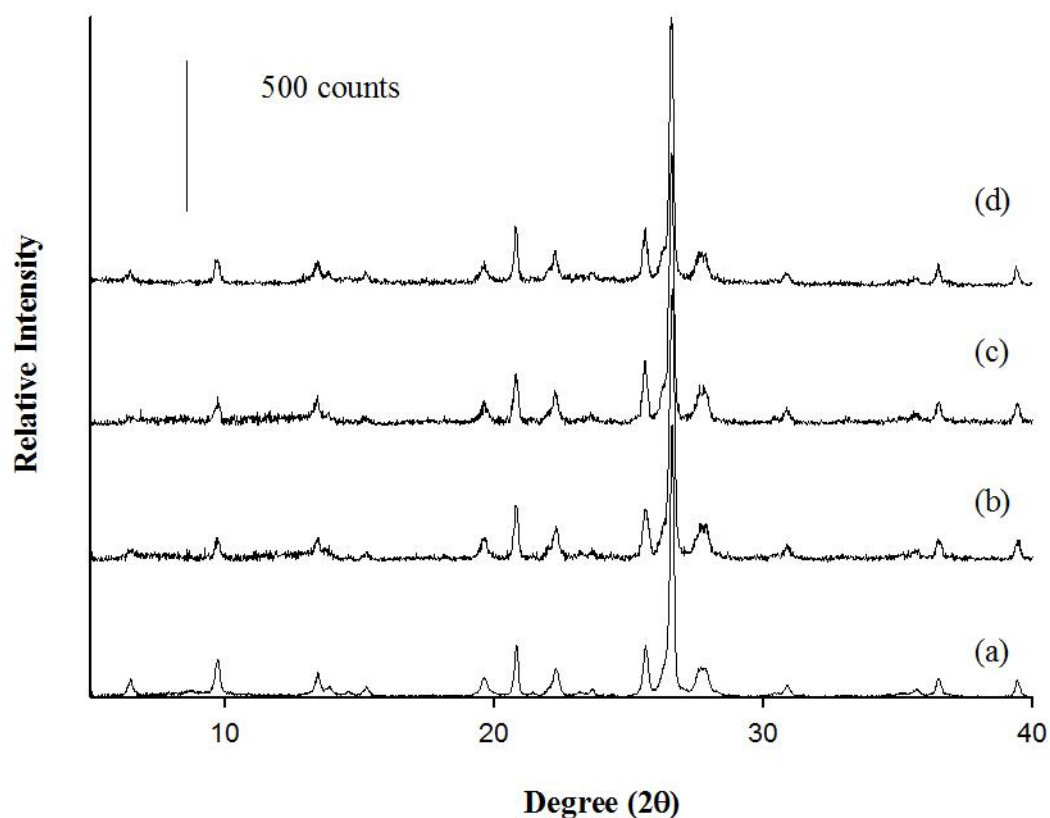


Figure 9. XRD patterns of (a) zeolite, and composites (b) COMP 20:1 (c) COMP 10:1 (d) COMP 5:1.

4.1.2 SEM/EDS Analysis

The morphology of zeolite and zeolite-xanthan gum composites was characterized by SEM technique. Figure 10 shows the micrograph of the activated mordenite which displays a rough heterogeneous surface morphology. In the micrograph, it can be observed zeolite particles with irregular forms and different sizes, ranging from few microns to particles larger than 20 μm . Also, it can be observed that some zeolite particles are forming agglomerates. The mentioned morphology is consistent with previously reported studies of mordenite^{60,61}.

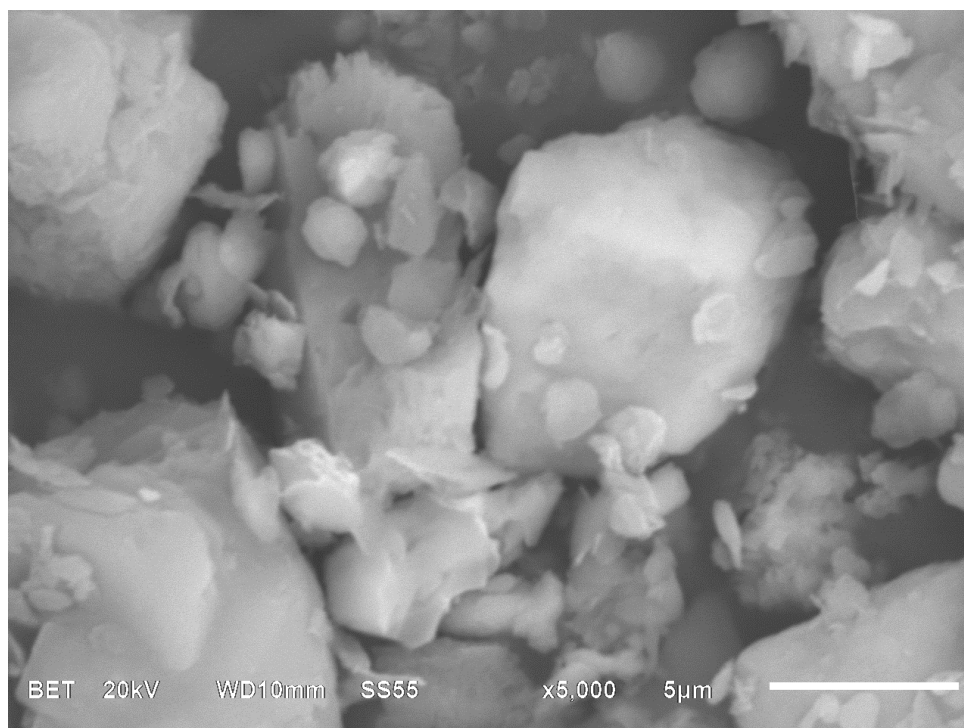


Figure 10. SEM micrograph of zeolite. (Magnification: 5000x)

Figure 11. shows the micrograph of composite Comp 20:1 and Comp 10:1 which reveals zeolite particles of different sizes and irregular shapes with a heterogeneous surface morphology.

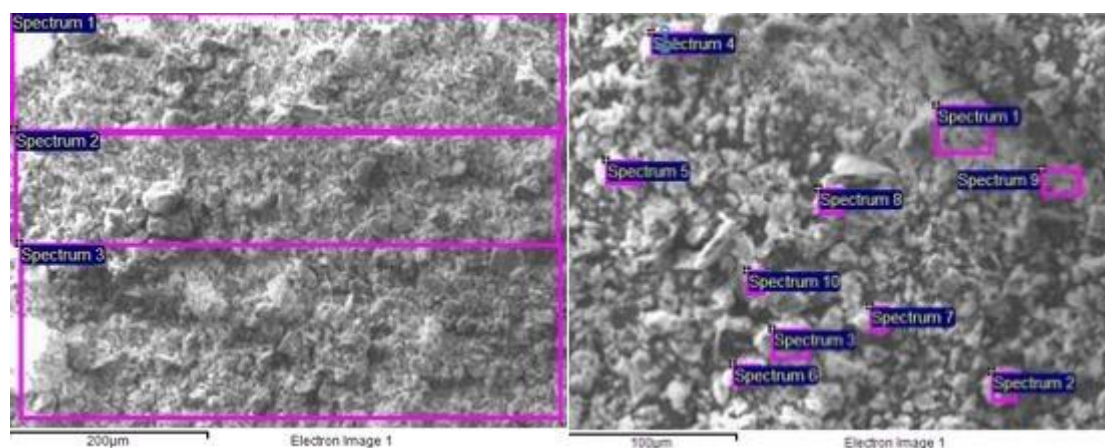


Figure 11. SEM micrograph of composite Comp 20:1 and Comp 10:1.

Results of the EDS analysis of the zeolite and zeolite-xanthan gum composites is shown in Figure 12. The results show that the zeolite has a Si/Al mole ratio of about 4.3, that is within the range of intermediate silica zeolites (Si/Al: 2 to 5)⁶² which is consistent

with the classification composition of mordenite ⁶². Moreover, Na⁺, K⁺, Ca²⁺ and Mg²⁺ are present in the natural mordenite structure, being Ca²⁺ the predominant exchangeable cation. On the other hand, the analysis reveals the presence of carbon in the composites while in zeolite it was completely absent, confirming that xanthan gum was successfully incorporated on the surface of zeolite.

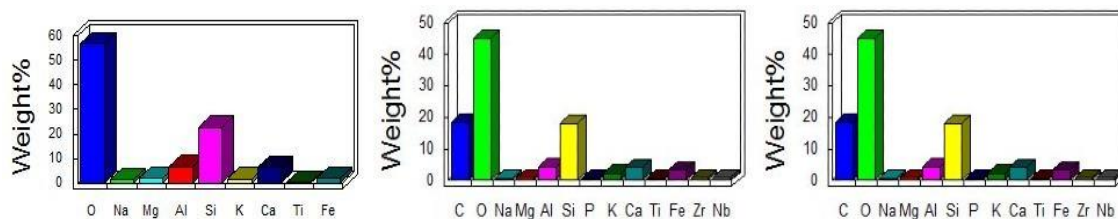


Figure 12. EDS for (a) zeolite and composites: (b) COMP 20:1, (c) COMP 10:1

4.1.3 Fourier Transform Infrared Spectroscopy (FTIR)

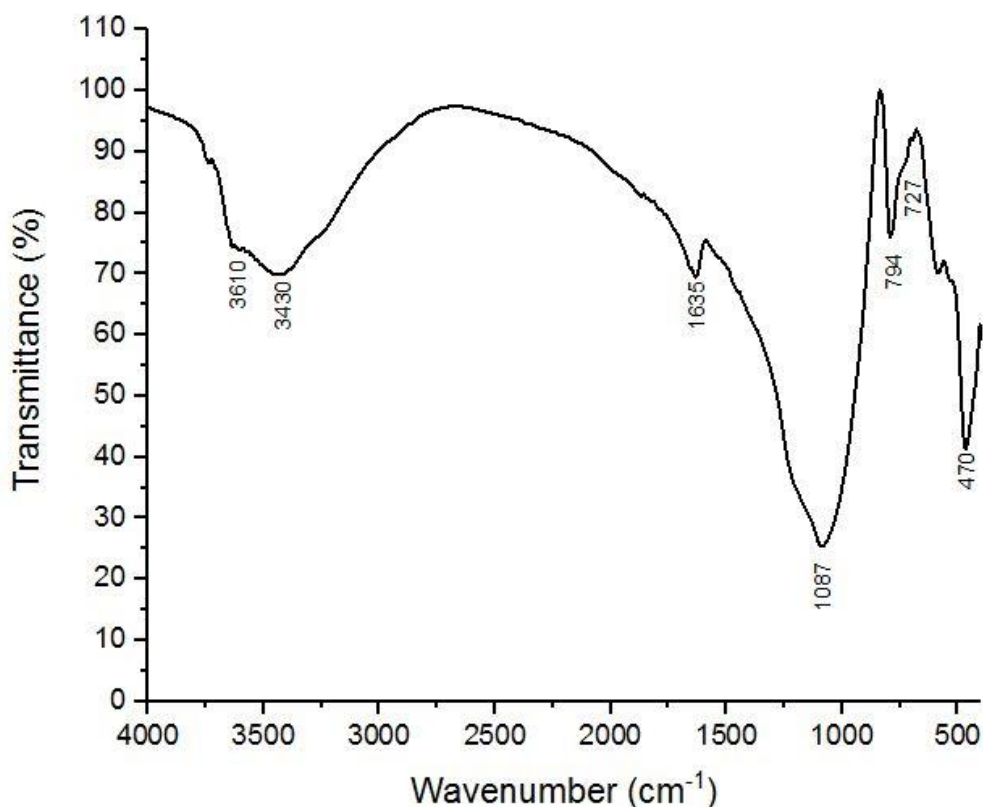


Figure 13. FTIR spectrum of the natural mordenite sample.

The FT-IR spectrum of mordenite is shown in Figure 13 in which the characteristic broad band between 3000 and 3650 cm^{-1} region is observed. In specific, the band at $\sim 3610 \text{ cm}^{-1}$ corresponds to the stretching vibrations of O-H of the silanol (Si-OH) groups, meanwhile the band at $\sim 3430 \text{ cm}^{-1}$ is attributed to the O-H stretching vibrations of adsorbed water. The sharp band observed at $\sim 1635 \text{ cm}^{-1}$ corresponds to the bending vibration of H-O-H⁶³. Additionally, a strong band appears at 1087 cm^{-1} which corresponds to asymmetric T-O stretching vibration in TO_4 tetrahedral (T = Si and Al), and its position depends on the content of framework Si and Al⁶⁴. The bands at 727 and 470 cm^{-1} are assigned to the symmetric stretching and bending modes of internal tetrahedra, respectively⁶⁵, while the band at 794 cm^{-1} corresponds to symmetric stretching mode of external linkages⁶⁶.

The infrared spectra of commercial xanthan gum is shown in Figure 14

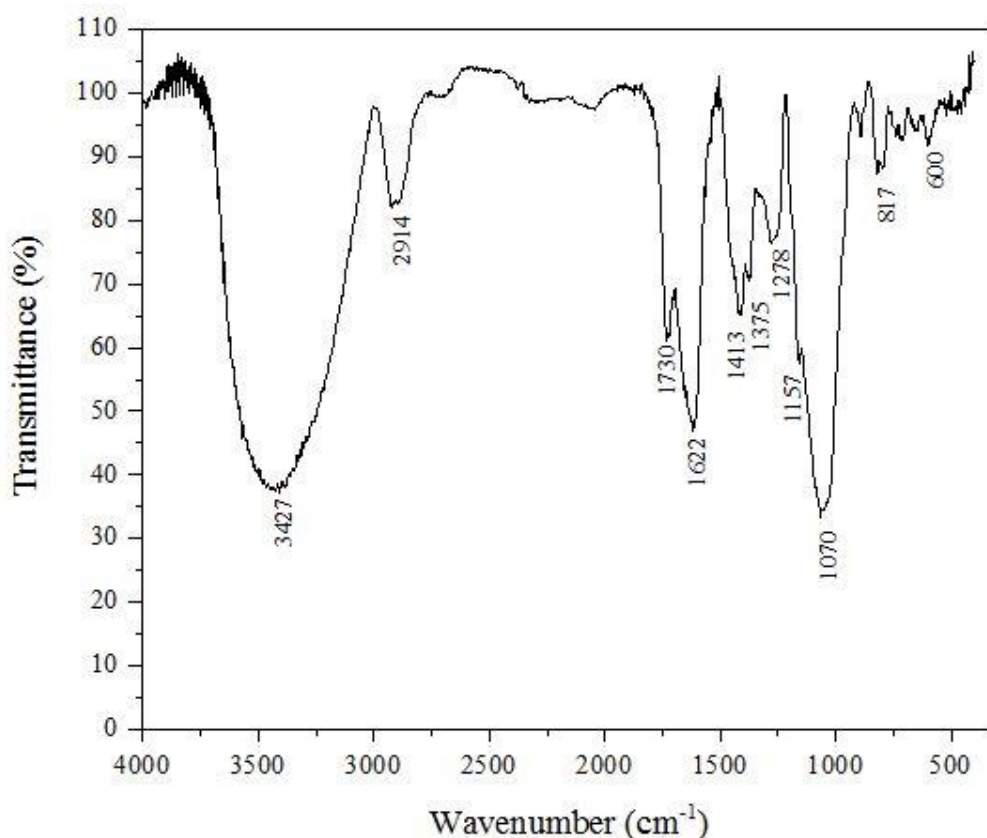


Figure 14. FTIR spectrum of xanthan gum.

The strong and wide band at 3427 cm^{-1} is attributed to O-H stretching vibrations, whereas the characteristic band at 2914 cm^{-1} is due to axial deformation of C-H of alkanes ($-\text{CH}_2-$). The signal at 1730 cm^{-1} corresponds to C=O stretch, and the signals at 1622 cm^{-1} and 1413 cm^{-1} are due to asymmetric and symmetric vibrations of COO^- in pyruvate and

glucuronate group⁶⁷. The presence of the peaks at 1157 and 1070 cm^{-1} correspond to C-O bending^{59,68}.

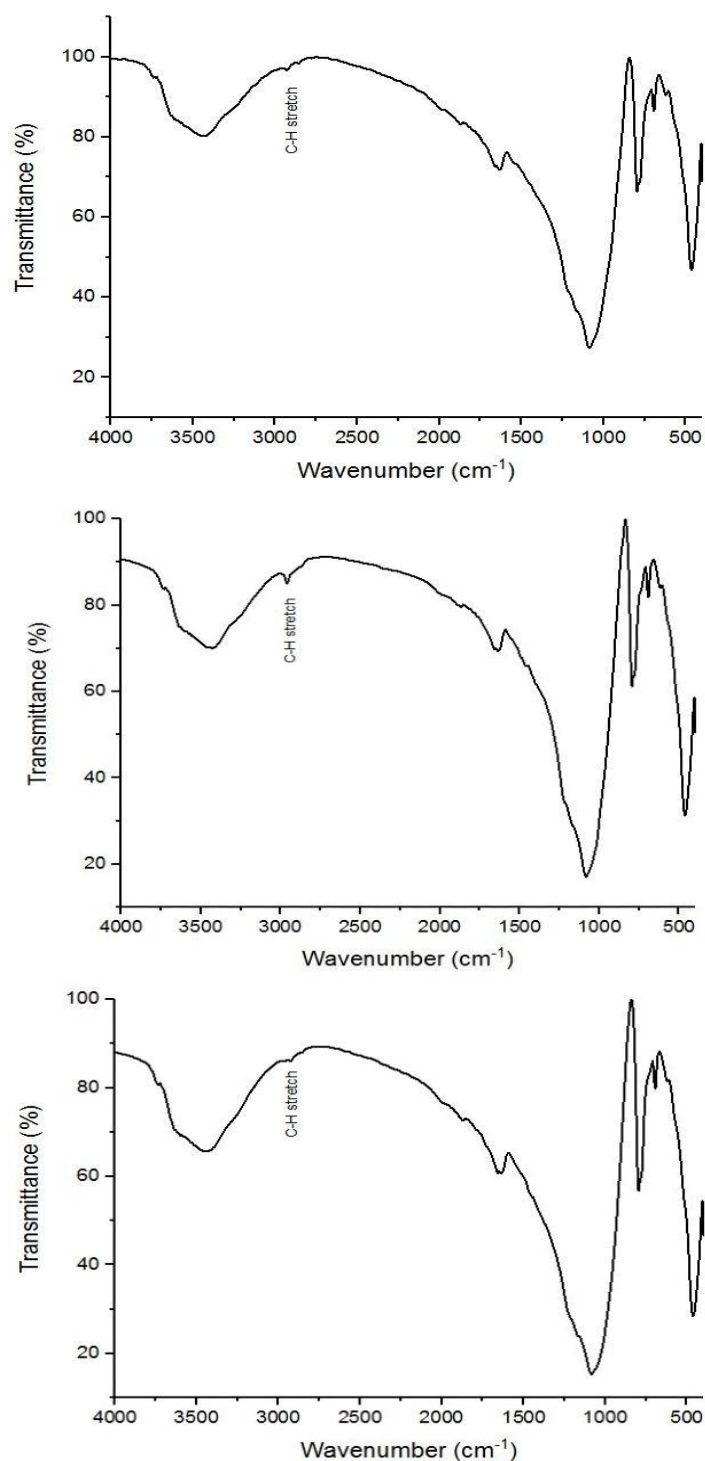


Figure 15. FTIR spectra of COMP 20:1, COMP 10:1, COMP 5:1

For the composites (Figure 15), in addition to the bands corresponding to zeolite, an extra band is observed around 2924 cm^{-1} which corresponds to C-H stretching vibrations. This

band is absent in the parental zeolite which confirms the presence of xanthan gum in the composites.

4.2 Adsorption

4.2.1 Effect of initial pH on chromium adsorption

The effect of pH on the adsorption capacity and removal of Cr(VI) onto zeolite and zeolite – xanthan gum composites was investigated by testing two values of pH: 2 and 9. The solution pH is one of the most important variables controlling the adsorption process. The dissociation of active functional groups of the adsorbent as well as the surface solids charge are influenced by pH variation^{20,69}.

According to Figure 16, the Cr(VI) removal efficiency is favored under acidic conditions (pH 2). A higher adsorption capacity of Cr(VI) by zeolite (1.23 mg/g), COMP 20:1 (1.89 mg/g), COMP 10:1 (2.18 mg/g) and COMP 5:1 (1.60 mg/g) was found at pH 2, however these values reduced to 0.48 mg/g, 0.63 mg/g, 0.70 mg/g and 0.54 mg/g, respectively, at pH 9.0. Several authors have also reported that adsorption of Cr(VI) onto hydrous solids and biocomposites increased with lowering of pH and it is highest at pH 2.0^{16,23}

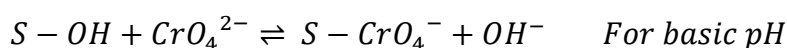
In aqueous solutions, Cr(VI) exists as five main species: H_2CrO_4 ; $HCrO_4^-$; CrO_4^{2-} ; $HCr_2O_7^-$; $Cr_2O_7^{2-}$ and their distribution depends on the total chromium concentration and the pH of the solution⁷⁰. At pH values between 2 and 6, $HCrO_4^-$ and $Cr_2O_7^{2-}$ chromium (VI) species appear together, although $HCrO_4^-$ predominates, and at higher pH (pH > 6) Cr(VI) only exists in the form of CrO_4^{2-} .⁷¹

The increase in adsorption capacity of Cr(VI) at pH 2.0 could be explained with the following schemes, where S represents the surface sites of the adsorbent, $S-OH_2^+$, $S-OH$ and $S-O^-$ refer to protonated, neutral and deprotonated surface hydroxyl functional groups, respectively.



At lower pH, as the concentration of H^+ ions increases, the hydroxyl functional groups of the zeolite surface are activated (protonated), consequently, coulombic interaction forces can exist between $HCrO_4^-$ anionic species and the activated surface sites²³. In addition, $(S-OH_2^+)$ becomes a good leaving group, and is most easily replaced with the $HCrO_4^-$ ions.

Figure 16 also shows that at pH 9, the removal percentages of Cr(VI) are very low. This can be explained due to at high pH values, the positively charged active sites of the adsorbent get decreased and its surface acquires a negative charge and hence, electrostatic repulsion takes place between the adsorbent and the Cr(VI) oxyanions. At basic pH, the neutral surface hydroxyl functional group (S-OH), may be the only active site available for CrO_4^{2-} adsorption. In addition, at basic region, there is an increasing amounts of hydroxyl ions (OH^-), which compete with chromate (CrO_4^{2-}) ions for occupying active sites in adsorbent pore²³.



In the case of zeolite-xantham gum composites, the active sites available for Cr(VI) adsorption not only include hydroxyl functional groups but also carboxyl, which are present on their surface.

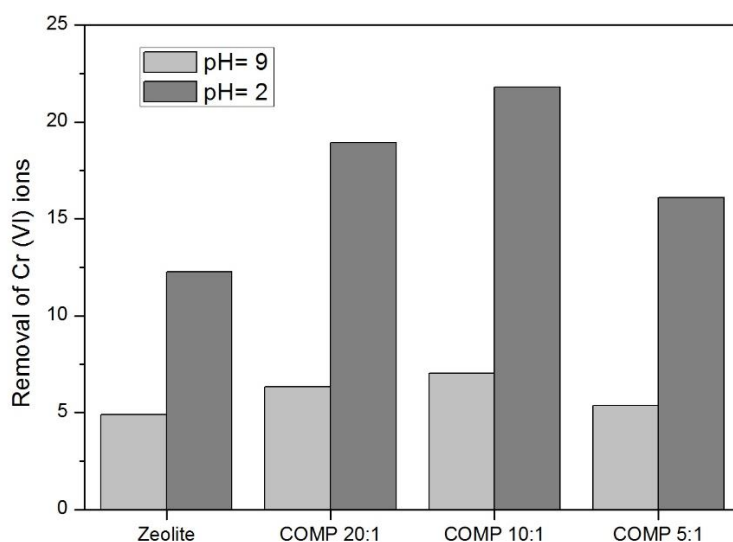


Figure 16. Effect of initial pH on Cr(VI) removal efficiency (adsorbent dosage: 10 g/L, initial Cr(VI) concentration: 100 mg/L and reaction time: 24 h)

4.2.2 Effect of contact time

The percentage of removal of Cr (VI) ions from aqueous solution by different adsorbents is showed in Figure 17. It may be seen that there was a slight increase in the removal percentage of Cr (VI) ions from 3 to 24 hours for all adsorbents. The adsorption capacity also increased at longer contact time. The longer the contact time, the greater is the probability for Cr(VI) ions to bind at the active sites on the adsorbent's surface⁶.

As can be observed in Figure 17, in most cases less than 8% of Cr(VI) ions were removed by using zeolite solely as adsorbent while zeolite-xanthan gum composites removed about 11.97% - 21.80%, indicating that the hybrid usage of both adsorbents improved the effectiveness for Cr(VI) removal. Zeolite cannot efficiently remove Cr(VI) because as most natural zeolites it possesses a net negative structural charge on its external surface which causes them to have little affinity for anions⁷². The achieved enhancement observed for zeolite-xanthan gum composites in the Cr(VI) uptake might be due to greater diversity of binding groups (hydroxyl and carboxyl) existing in their surface which act as potential available sites for Cr(VI) adsorption at pH=2.

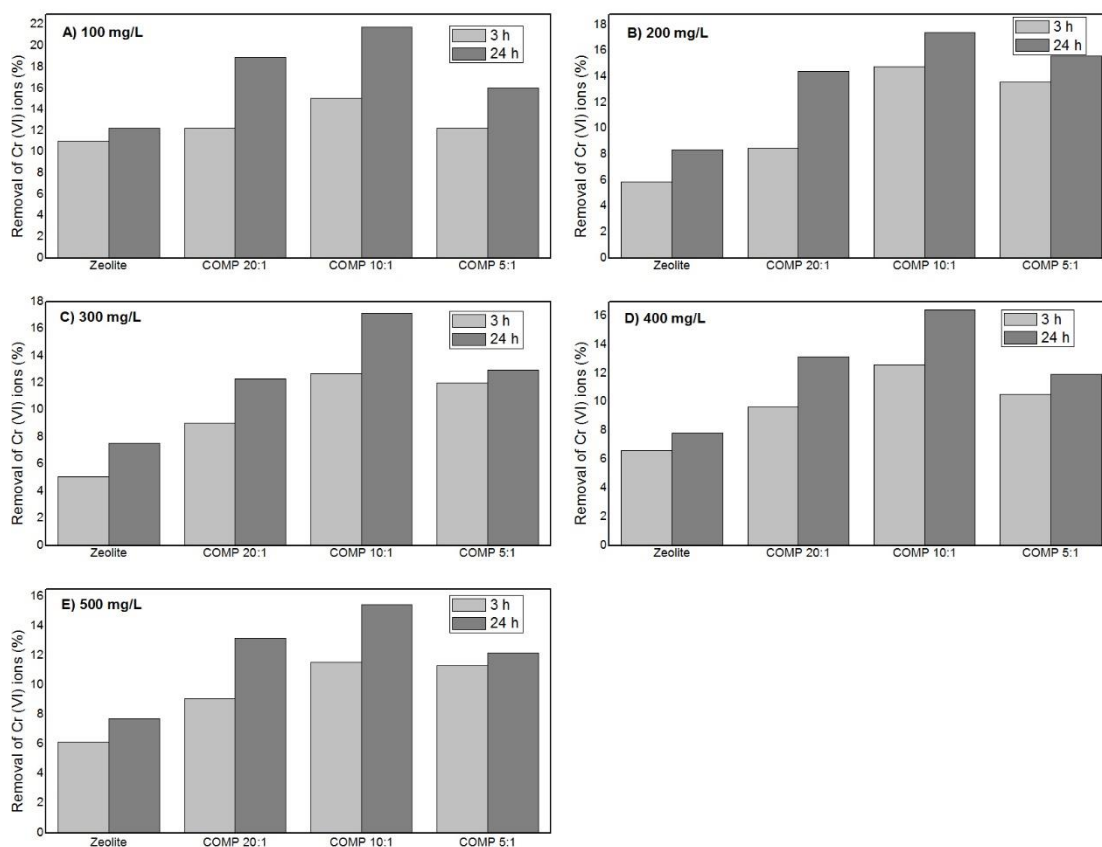


Figure 17. Percentage of removal of Cr (VI) ions by zeolite, COMP(5:1), COMP(10:1) and COMP(20:1) as a function of time. (Initial Cr(VI) concentration: (A) 100 mg/L, (B) 200 mg/L, (C) 300 mg/L, (D) 400 mg/L, (E) 500 mg/L, adsorbent dosage: 10 g/L, and pH: 2)

4.2.3 Effect of initial concentration

The removal efficiency of Cr(VI) decreased with increase in Cr(VI) concentration for all adsorbents. On the other hand, Cr(VI) adsorption capacity increased along with the Cr(VI) concentration increase from 100 to 500 mg/L (Figure 18). The maximum Cr(VI) adsorption capacity was found at 500 mg/L indicating that initial concentration of chromium solution have a significant impact in adsorption, which means that greater solute uptake can be obtained from higher concentrations. This can be explained due to the higher the initial concentration, the greater the number of Cr(VI) ions reaching the active sites of the adsorbent surface, that is, the probability of interaction between Cr(VI) ions and active sites increases at higher concentrations.

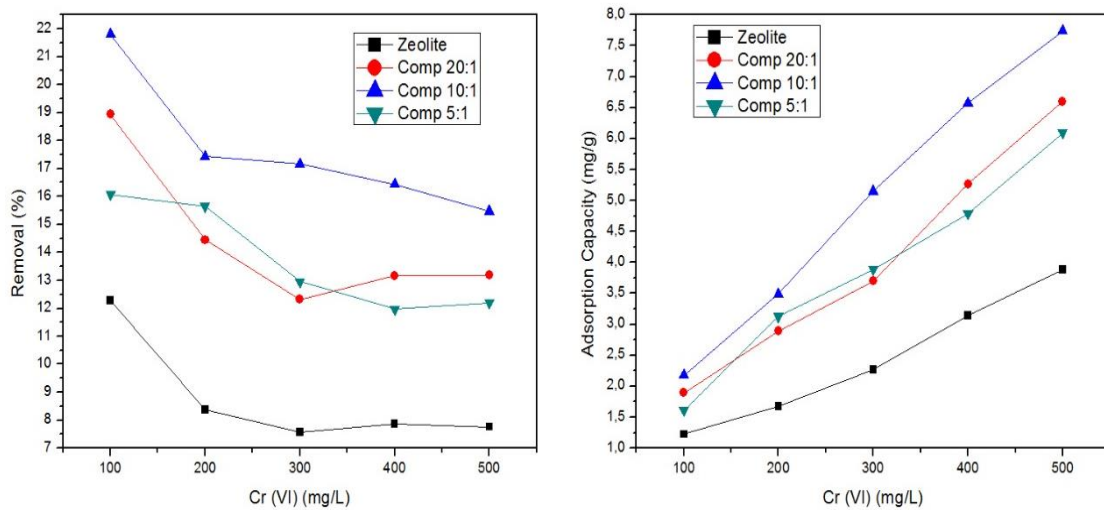


Figure 18. Effect of the initial Cr(VI) concentration (100 - 500 mg/L) in the adsorption capacity (mg/g) and removal efficiency (R %) of Cr(VI) ions (adsorbent dosage: 10 g/L, pH: 2 and reaction time: 24 h).

4.2.4 Adsorption isotherms

Langmuir, Freundlich, and Temkin isotherms were used as model to be fitted to the experimental data. The study of isotherm models was carried out in pH of the solution,

adsorbent dosage, and contact time of 2, 10 g/L, and 24 hours, respectively. The parameters of the studied isotherms are presented in the Table 4.

The best-fit model was selected based on correlation coefficient (R^2). For all adsorbent materials, it may be seen that the Freundlich isotherm of adsorption model (Figure 19) better described the experimental data than Langmuir and Temkin models. The Freundlich isotherm indicates that the adsorption mechanism of Cr(VI) on zeolite and zeolite-xanthan gum composites involves a reversible adsorption-desorption process due to adsorbent-adsorbate weak interactions. Also, it suggests a heterogeneous distribution of active adsorbent surface sites. The values of Freundlich n parameter for each adsorbent is > 1 which expresses favorable adsorption processes.

Table 4. Isotherm parameters for Cr(VI) adsorption onto zeolite and zeolite-xanthan gum composites.

Isotherm model	Parameters	Adsorbent			
		Mordenite	COMP(20:1)	COMP(10:1)	COMP(5:1)
Langmuir	Q_{\max} (mg/g)	9,033	16,500	20,948	15,017
	K_L (L/mg)	0,001	0,001	0,001	0,001
	R^2	0,613	0,589	0,851	0,872
	R_L	0,58 -0,87	0,60 - 0,88	0,59-0,88	0,58-0,87
Freundlich	K_f (mg/g)	0,051	0,072	0,074	0,055
	n	1,442	1,371	1,303	1,301
	R^2	0,956	0,967	0,994	0,987
Temkin	B (mg/g)	1,541	2,649	3,298	2,520
	K_T (L/mg)	0,020	0,021	0,021	0,021
	R^2	0,875	0,878	0,948	0,956

The maximum adsorption capacity was of 0.051 mg/g for zeolite, 0.072 mg/g for COMP(20:1), 0.074 mg/g for COMP(10:1), and 0.055 mg/g for COMP(5:1). The obtained results showed that composites have higher adsorption capacity than zeolite. This can be explained by the greater diversity of active functional groups present on the surface of composites which can form complexes with Cr(VI) anions. Furthermore, among the studied composites, the composite formed with the ratio zeolite: xanthan gum (10:1) was the best hybrid proportion with an adsorption capacity of 0.074 mg/g. Increasing the amount of xanthan gum in the ratio of adsorbent (COMP 5:1) did not improve the Cr(VI) adsorption capacity. The reason might be because the excess of xanthan gum polysaccharide can block the porous structure of the composite ¹⁸ reducing the available sites for targeted metal ion adsorption.

The scientific literature gives no previous data of removal of Cr(VI) by zeolite-xanthan gum composites. There are some articles reporting hybrid composites based on xanthan gum with synthetic zeolites for removal of Co²⁺, Ni²⁺ ¹⁸ Pb²⁺ and anionic dye ¹⁷. The comparison of Cr(VI) adsorption capacity of various adsorbents that have been reported in literature is presented in Table 5. It can be seen that the present composites do not exhibit sufficient adsorption capacity among other hybrid adsorbents reported earlier.

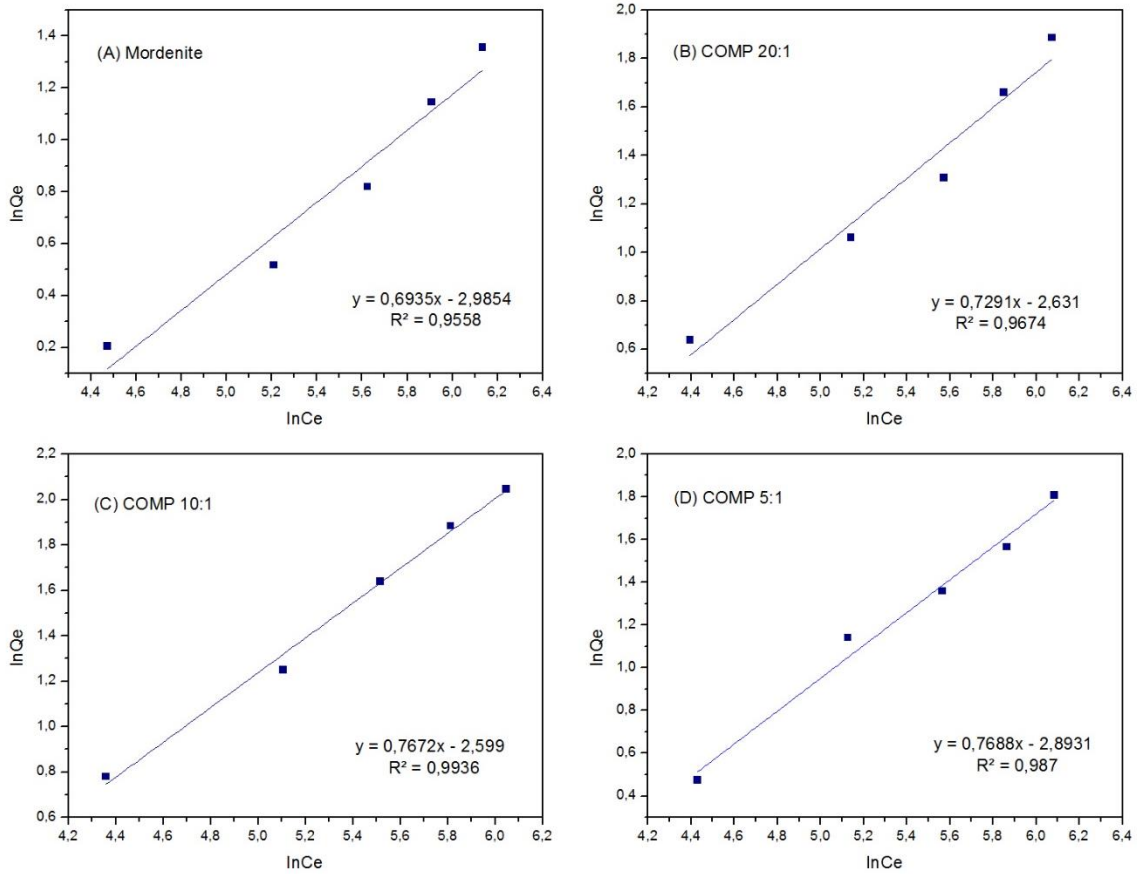


Figure 19. Linear plot of Freundlich isotherm for the adsorption of Cr(VI) ions on (A) Zeolite, (B) COMP 20:1, (C) COMP 10:1 and (D) COMP 5:1 (adsorbent dosage: 10 g/L, Initial Cr(VI) solution concentration: 100 – 500 mg/L, pH: 2 and reaction time: 24 h)

Table 5. Maximum adsorption capacity of various adsorbents for Cr(VI) removal from aqueous solutions

Adsorbent	pH	Isotherm	Maximum adsorption Capacity (mg/g)	Reference
Natural Clinoptilolite Zeolite	2	Freundlich	1.193	23
Natural Clinoptilolite Zeolite from Greece	4	Langmuir	4.12	73
Brown coal	-	Langmuir	0.314	28
Modified zeolite	-	Freundlich	0.873	
Zeolite/Chitosan hybrid composite	4	Langmuir	0.109	16

Crosslinked chitosan- diethylenetriaminepentaacetic acid	3	Langmuir	192.3	74
Sulphate-crosslinked chitosan (SCC)	3	Langmuir	250.90	75
Opuntia Biomass	2	Langmuir and Freundlich	16.4 - 18.5	76
Biomass material	4	Langmuir	227.3	77
Zeolite: Xanthan gum (10:1)	2	Freundlich	0,074	Current study

CHAPTER 5

CONCLUSION

5.1 Conclusion

In this study, three zeolite-xanthan gum composites were successfully prepared and characterized using various techniques including SEM/EDS, FTIR, and DRX. The capability of activated mordenite zeolite and zeolite-xanthan gum composites was studied for Cr(VI) adsorption in aqueous solutions. It was found that Cr(VI) adsorption on all adsorbents was highly pH dependent. At pH 2, a higher removal efficiency was obtained due to an acidic condition, a surface coordination process can take place between the activated functional groups of adsorbent surface and Cr(VI) ions. The adsorption results showed that the Cr(VI) adsorption capacity of the activated zeolite enhanced by functionalizing it with xanthan gum. The composite formed with the ratio zeolite: xanthan gum (10:1) was the best hybrid proportion which showed an adsorption capacity of 0.074 mg/g. The experimental data was analyzed by using Langmuir, Freundlich and Temkin isotherms. The Freundlich isotherm model was best fitted to the adsorption of Cr(VI) on all adsorbents, indicating a heterogeneous distribution of active adsorbent surface sites. Additionally, the adsorption process involves reversible physisorption as a result of adsorbent-adsorbate weak interactions.

5.2 Suggestions for future work

Although the objectives of this study were achieved, there are some other aspects that were not investigated due to the limitations of time and equipment's availability. Therefore, additional research is needed in order to obtain a wider perspective for possible applications. Some recommendations for further studies are given below:

- In this research, the effect of pH, contact time and initial concentration on the Cr(VI) adsorption was evaluated, while the effect of other parameters such as effect of temperature, stirring rate, adsorbent mass and adsorbent particle size was not included. However, as these parameters act together in solution, they need to be studied.

- Also, in this work, only isotherm studies were conducted. In order to evaluate the feasibility and viability of sorption process, kinetic and thermodynamic studies could be performed.
- This study has only focused on the removal of Cr(VI) anions from synthetic solutions. However, the adsorption capacity of natural zeolite for cations such as Cu^{2+} , Pb^{2+} , Ni^{2+} , Fe^{3+} and Zn^{2+} can be investigated in order to determine whether the studied adsorbents can efficiently remove cations from aqueous solutions.

REFERENCES

1. PIMENTEL, D. *et al.* Water Resources: Agricultural and Environmental Issues. *Bioscience* **54**, 909 (2004).
2. Brownlie, W. J. *et al.* Freshwater science for the benefit of society: a perspective from early career researchers. *Int. Waters* **7**, 227–235 (2017).
3. Jorgetto, A. D. O. *et al.* Multilayer adsorption of Cu(II) and Cd(II) over Brazilian Orchid Tree (Pata-de-vaca) and its adsorptive properties. *Appl. Surf. Sci.* **345**, 81–89 (2015).
4. Meena, A. K., Mishra, G. K., Rai, P. K., Rajagopal, C. & Nagar, P. N. Removal of heavy metal ions from aqueous solutions using carbon aerogel as an adsorbent. *J. Hazard. Mater.* **122**, 161–170 (2005).
5. Tchounwou, P. B., Yedjou, C. G., Patlolla, A. K. & Sutton, D. J. Heavy metal toxicity and the environment. *EXS* **101**, 133–164 (2012).
6. Agustina, T. E., Aprianti, T. & Miskah, S. Treatment of wastewater containing hexavalent chromium using zeolite ceramic adsorbent in adsorption column. *Int. J. Adv. Sci. Eng. Inf. Technol.* **7**, 566–572 (2017).
7. Masindi, V. & Muedi, K. L. Environmental Contamination by Heavy Metals. in *Heavy Metals* (2018). doi:10.5772/intechopen.76082
8. Ertugay, N. & Bayhan, Y. K. Biosorption of Cr (VI) from aqueous solutions by biomass of *Agaricus bisporus*. *J. Hazard. Mater.* **154**, 432–439 (2008).
9. Medina, M. & Pozo, P. Determinación de cromo hexavalente en descargas de aguas residuales de una curtiembre, ubicada en el sector de Izamba, Ambato en la provincia de Tungurahua, mediante espectrofotometría de absorción atómica. *infoANALÍTICA* **1**, (2013).
10. Maestu, J. *10 year Water for Life*. (2015).
11. Ministerio del Ambiente. Anexo 1 Del Libro Vi Del Texto Unificado De Legislacion Secundaria Del Ministerio Del Ambiente: Norma De Calidad Ambiental Y De Descarga De Efluentes Al Recurso Agua. *Norma Calid. Ambient. Y Descarga Efluentes Recur. Agua* 1–37 (2014).
12. Pandey, P., Sambhi, S. S., Sharma, S. K. & Singh, S. Batch Adsorption Studies for the Removal of Cu(II) Ions by ZeoliteNaX from Aqueous Stream. *Lect. Notes Eng. Comput. Sci.* **2178**, 122–127 (2009).
13. Guo, Z., Zhang, X., Kang, Y. & Zhang, J. Biomass-Derived Carbon Sorbents for

- Cd(II) Removal: Activation and Adsorption Mechanism. *ACS Sustain. Chem. Eng.* **5**, 4103–4109 (2017).
14. Misaelides, P. Application of natural zeolites in environmental remediation: A short review. *Microporous Mesoporous Mater.* **144**, 15–18 (2011).
 15. Shaheen, S. M., Derbalah, A. S. & Moghanm, F. S. Removal of Heavy Metals from Aqueous Solution by Zeolite in Competitive Sorption System. *Int. J. Environ. Sci. Dev.* 362–367 (2012). doi:10.7763/ijesd.2012.v3.248
 16. Meiling Pang, Naoki Kano & Hiroshi Imaizumi. Adsorption of Chromium (VI) from Aqueous Solution Using Zeolit/Chitosan Hybrid Composite. *J. Chem. Chem. Eng.* **9**, (2015).
 17. Ahmad, R. & Mirza, A. Adsorptive removal of heavy metals and anionic dye from aqueous solution using novel Xanthan gum-Glutathione/ Zeolite bionanocomposite. *Groundw. Sustain. Dev.* **7**, 305–312 (2018).
 18. Zhang, W., Xu, F., Wang, Y., Luo, M. & Wang, D. Facile control of zeolite NaA dispersion into xanthan gum-alginate binary biopolymer network in improving hybrid composites for adsorptive removal of Co²⁺ and Ni²⁺. *Chem. Eng. J.* **255**, 316–326 (2014).
 19. Rengaraj, S., Yeon, K. H. & Moon, S. H. Removal of chromium from water and wastewater by ion exchange resins. *J. Hazard. Mater.* **87**, 273–287 (2001).
 20. Kučić, D., Simonic, M. & Furac, L. Batch adsorption of Cr(VI) ions on zeolite and agroindustrial waste. in *Chemical and Biochemical Engineering Quarterly* **31**, 497–507 (2018).
 21. MacIngova, E. & Luptakova, A. Recovery of metals from acid mine drainage. in *Chemical Engineering Transactions* **28**, 109–114 (2012).
 22. Aksu, Z., Gönen, F. & Demircan, Z. Biosorption of chromium(VI) ions by Mowital®B30H resin immobilized activated sludge in a packed bed: Comparison with granular activated carbon. *Process Biochem.* **38**, 175–186 (2002).
 23. Jorfi, S. *et al.* Adsorption of Cr(VI) by Natural Clinoptilolite Zeolite from Aqueous Solutions: Isotherms and Kinetics. *Polish J. Chem. Technol.* **19**, 106–114 (2017).
 24. Siddiqui, V. U. *et al.* Nanographene composite ion exchanger properties and applications. in *Nanocarbon and its Composites* 629–649 (2019). doi:10.1016/b978-0-08-102509-3.00021-3
 25. Inglezakis, V. J. & Grigoropoulou, H. P. Applicability of simplified models for the estimation of ion exchange diffusion coefficients in zeolites. *J. Colloid Interface Sci.*

- 234**, 434–441 (2001).
26. Bansal, R. C. & Goyal, M. *Activated carbon adsorption. Activated Carbon Adsorption* (2005). doi:10.1680/bwtse.63341.147
 27. García Asenjo, N. Una Nueva Generación De Carbones Activados De Altas Prestaciones Para Aplicaciones Medioambientales. *Univ. Oviedo* 217 (2014).
 28. Akbari Binabaj, M., Nowee, S. M. & Ramezani, N. Comparative study on adsorption of chromium(VI) from industrial wastewater onto nature-derived adsorbents (brown coal and zeolite). *Int. J. Environ. Sci. Technol.* **15**, 1509–1520 (2018).
 29. Ho, Y. S. & McKay, G. The kinetics of sorption of divalent metal ions onto sphagnum moss peat. *Water Res.* **34**, 735–742 (2000).
 30. Langmuir, I. The constitution and fundamental properties of solids and liquids. Part I. Solids. *J. Am. Chem. Soc.* **38**, 2221–2295 (1916).
 31. Liang, S., Guo, X., Feng, N. & Tian, Q. Isotherms, kinetics and thermodynamic studies of adsorption of Cu²⁺ from aqueous solutions by Mg²⁺/K⁺ type orange peel adsorbents. *J. Hazard. Mater.* **174**, 756–762 (2010).
 32. Behnamfard, A. & Salarirad, M. M. Equilibrium and kinetic studies on free cyanide adsorption from aqueous solution by activated carbon. *J. Hazard. Mater.* **170**, 127–133 (2009).
 33. Kučić, D., Čosić, I., Vuković, M. & Briški, F. Sorption kinetic studies of ammonium from aqueous solution on different inorganic and organic media. *Acta Chim. Slov.* **60**, 109–119 (2013).
 34. Jain, M., Garg, V. K. & Kadirvelu, K. Equilibrium and kinetic studies for sequestration of Cr(VI) from simulated wastewater using sunflower waste biomass. *J. Hazard. Mater.* **171**, 328–334 (2009).
 35. H.M.F. Freundlich. Über die adsorption in losungen, *Z. Phys. Chem.* **57A**, 385–470 (1906).
 36. Gottardi, G. & Galli, E. *Natural Zeolites. Natural Zeolites* (Springer-Verlag Berlin Heidelberg, 1985). doi:10.1007/978-3-642-46518-5
 37. Clifton, R. A. *NATURAL AND SYNTHETIC ZEOLITES. Information Circular - United States, Bureau of Mines* (1987).
 38. Auerbach, S., Carrado, K. & Dutta, P. *Handbook of Zeolite Science and Technology. Handbook of Zeolite Science and Technology* (Marcel-Dekker, 2003). doi:10.1201/9780203911167

39. Ghobarkar, H., Schäf, O. & Guth, U. Zeolites - from kitchen to space. *Progress in Solid State Chemistry* **27**, 29–73 (1999).
40. Mumpton, F. A. La roca magica: Uses of natural zeolites in agriculture and industry. *Proc. Natl. Acad. Sci. U. S. A.* **96**, 3463–3470 (1999).
41. Baerlocher, C., McCusker, L. B. & Olson, D. H. *Atlas of Zeolite Framework Types, 6th Edition. Atlas of Zeolite Framework Types* (2007). doi:10.1016/B978-044453064-6/50287-5
42. Armbruster, T. & Gunter, M. E. Crystal structures of natural zeolites. *Rev. Mineral. Geochemistry* **45**, 1–67 (2001).
43. Ruren, X., Wenqin, P., Jihong, Y., Qisheng, H. & Jiesheng, C. *Chemistry of Zeolites and Related Porous Materials. Chemistry of Zeolites and Related Porous Materials* (2007). doi:10.1002/9780470822371
44. Margeta, K., Zabukovec, N., Siljeg, M. & Farkas, A. Natural Zeolites in Water Treatment – How Effective is Their Use. in *Water Treatment* (2013). doi:10.5772/50738
45. Szerement, J., Ambrożewicz-Nita, A., Kędziora, K. & Piasek, J. Use of Zeolite in Agriculture and Environmental Protection . A Short Review. *Dep. Phys. Chem. Porous Mater.* 172–177 (2014). doi:10.1523/jneurosci.4327-05.2006
46. Inglezakis, V. J. & Zorpas, A. A. *Handbook of natural zeolites. Handbook of Natural Zeolites* (2012). doi:10.2174/97816080526151120101
47. Dyer, A. Chapter 14 - Ion exchange capacity. in *Verified Syntheses of Zeolitic Materials* 67–68 (2001). doi:http://dx.doi.org/10.1016/B978-044450703-7/50112-5
48. Colella, C. Natural zeolites. in *Studies in Surface Science and Catalysis* **157**, 13–40 (2005).
49. García-Ochoa, F., Santos, V. E., Casas, J. A. & Gómez, E. Xanthan gum: Production, recovery, and properties. *Biotechnol. Adv.* **18**, 549–579 (2000).
50. Sworn, G. Xanthan gum. in *Handbook of Hydrocolloids: Second Edition* 186–203 (2009). doi:10.1533/9781845695873.186
51. Holzwarth, G. & Prestridge, E. B. Multistranded helix in xanthan polysaccharide. *Science (80-.)*. **197**, 757–759 (1977).
52. Palaniraj, A. & Jayaraman, V. Production, recovery and applications of xanthan gum by *Xanthomonas campestris*. *Journal of Food Engineering* **106**, 1–12 (2011).
53. Katzbauer, B. Properties and applications of xanthan gum. *Polym. Degrad. Stab.* **59**, 81–84 (1998).

54. Epp, J. X-Ray Diffraction (XRD) Techniques for Materials Characterization. in *Materials Characterization Using Nondestructive Evaluation (NDE) Methods* 81–124 (2016). doi:10.1016/B978-0-08-100040-3.00004-3
55. Yang, L. *Materials Characterisation: Introduction to Microscopic and Spectroscopic Methods. Materials Characterization* (2008). doi:10.1002/9780470823002.ch2
56. Khan, S. A. *et al.* Fourier transform infrared spectroscopy: Fundamentals and application in functional groups and nanomaterials characterization. in *Handbook of Materials Characterization* 317–344 (2018). doi:10.1007/978-3-319-92955-2_9
57. Smith, B. The Basics of Infrared Interpretation. in *Infrared Spectral Interpretation* 1–29 (2018). doi:10.1201/9780203750841-1
58. Bastardo-González, E., Deyán, C. C. & Brito, J. L. Acid activated pillared clays with aluminum as CoMo catalysts support for the hydrodesulphurization of thiophene. *Rev. Tec. la Fac. Ing. Univ. del Zulia* **41**, 95–103 (2018).
59. Al-Yasiri, M., Awad, A., Pervaiz, S. & Wen, D. Influence of silica nanoparticles on the functionality of water-based drilling fluids. *J. Pet. Sci. Eng.* **179**, 504–512 (2019).
60. Guesh, K., López-Muñoz, M. J., Márquez-Álvarez, C., Chebude, Y. & Diaz, I. Ethiopian natural zeolites for photocatalysis. *Bull. Chem. Soc. Ethiop.* **29**, 431–440 (2015).
61. Sakizci, M. & Özgül Tanriverdi, L. Influence of acid and heavy metal cation exchange treatments on methane adsorption properties of mordenite. *Turkish J. Chem.* **39**, 970–983 (2015).
62. Marakatti, V. DESIGN OF SOLID ACID CATALYSTS FOR PRINS REACTION AND TOLUENE DESIGN OF SOLID ACID CATALYSTS FOR PRINS. (Université Catholique de Louvain -, 2015).
63. Favvas, E. P. *et al.* Clinoptilolite, a natural zeolite material: Structural characterization and performance evaluation on its dehydration properties of hydrocarbon-based fuels. *Microporous Mesoporous Mater.* **225**, 385–391 (2016).
64. Doula, M. K. Synthesis of a clinoptilolite-Fe system with high Cu sorption capacity. *Chemosphere* **67**, 731–740 (2007).
65. Mansouri, N., Rikhtegar, N., Ahmad Panahi, H., Atabi, F. & Shahraki, B. K. Porosity, characterization and structural properties of natural zeolite - Clinoptilolite - As a sorbent. *Environ. Prot. Eng.* **39**, 139–152 (2013).
66. Yan, Y. *et al.* Structural characterization, adsorption and catalysis of FER-type zeolite synthesized in TMEDA-Na₂O-Al₂O₃-SiO₂-H₂O system. in *Proc Int Zeolite*

- Conf 12th 3*, 1991–1999 (1999).
67. Lal, N., Dubey, J., Gaur, P., Verma, N. & Verma, A. Chitosan based in situ forming polyelectrolyte complexes: A potential sustained drug delivery polymeric carrier for high dose drugs. *Mater. Sci. Eng. C* **79**, 491–498 (2017).
 68. Faria, S. *et al.* Characterization of xanthan gum produced from sugar cane broth. *Carbohydr. Polym.* **86**, 469–476 (2011).
 69. Malkoc, E., Nuhoglu, Y. & Dundar, M. Adsorption of chromium(VI) on pomace-An olive oil industry waste: Batch and column studies. *J. Hazard. Mater.* **138**, 142–151 (2006).
 70. Cabatingan, L. K., Agapay, R. C., Rakels, J. L. L., Ottens, M. & Van der Wielen, L. A. M. Potential of biosorption for the recovery of chromate in industrial wastewaters. *Ind. Eng. Chem. Res.* **40**, 2302–2309 (2001).
 71. Tandon, R. K., Crisp, P. T., Ellis, J. & Baker, R. S. Effect of pH on chromium(VI) species in solution. *Talanta* **31**, 227–228 (1984).
 72. Faghihian, H. & Bowman, R. S. Adsorption of chromate by clinoptilolite exchanged with various metal cations. *Water Res.* **39**, 1099–1104 (2005).
 73. Álvarez-Ayuso, E., García-Sánchez, A. & Querol, X. Purification of metal electroplating waste waters using zeolites. *Water Res.* **37**, 4855–4862 (2003).
 74. Bhatt, R., Sreedhar, B. & Padmaja, P. Adsorption of chromium from aqueous solutions using crosslinked chitosan-diethylenetriaminepentaacetic acid. *Int. J. Biol. Macromol.* **74**, 458–466 (2015).
 75. Shekhawat, A., Kahu, S., Saravanan, D. & Jugade, R. Synergistic behaviour of ionic liquid impregnated sulphate-crosslinked chitosan towards adsorption of Cr(VI). *Int. J. Biol. Macromol.* **80**, 615–626 (2015).
 76. Fernández-López, J. A., Angosto, J. M. & Avilés, M. D. Biosorption of hexavalent chromium from aqueous medium with opuntia biomass. *Sci. World J.* **2014**, (2014).
 77. Zhong, Q. Q., Yue, Q. Y., Gao, B. Y., Li, Q. & Xu, X. A novel amphoteric adsorbent derived from biomass materials: Synthesis and adsorption for Cu(II)/Cr(VI) in single and binary systems. *Chem. Eng. J.* **229**, 90–98 (2013).